



A novel resonant parametric feedback controller (RPFC) for suppressing nonlinear resonances and chaos in a cantilever beam

Swapnil Mahadev Dhobale · Shyamal Chatterjee

Received: 10 May 2023 / Accepted: 22 October 2023 / Published online: 24 November 2023
© The Author(s), under exclusive licence to Springer Nature B.V. 2023

Abstract This paper presents a novel resonant parametric feedback controller (RPFC) for suppressing nonlinear resonances and chaos in a cantilever beam using acceleration feedback. The excitation of the system may be due to 1:1 direct excitation, 1:3 subharmonic direct excitation, 3:1 superharmonic direct excitation, 1:2 parametric excitation, 1:4 subharmonic parametric excitation, self excitations, and combinations of two or more of these. The controller is designed in two stages. First, the measured acceleration signal of the beam is feedback to a second-order filter. Subsequently, the states of the second-order filter are used to formulate the nonlinear control function that is applied to the structure as a parametric input such that the controlled parametric variation produces dissipative force at the resonance. The analysis of the system is carried out using the method of multiple time-scales. A number of special cases demonstrating the efficacy of the controller in suppressing various nonlinear resonances and their combinations are studied. Finally, a novel frequency adaptation law is proposed to deal with the uncertainty in the system's natural frequency. The results are verified by numerical simulations and some experiments. Though the analysis is carried out for an

SDOF system, the proposed control scheme can easily be extended to any MDOF system, and it can target any mode by tuning the filter frequency.

Keywords Vibration · Active vibration control · Resonant controller · Parametric feedback · Adaptive control

1 Introduction

Flexible structures are susceptible to large deflections when excited at lower modes. The sources of excitations can be categorized into three main types: direct excitation, parametric excitation, and self-excitation. In the case of direct excitation, the system is subjected to time-dependent force. In the case of parametric excitation, the system gets excited due to variations in parameters with time. Mathieu first modeled the most straightforward parametrically excited system without any nonlinearities [1]. The non-dimensional equation of a base-excited cantilever beam with tip mass is similar to the Mathieu equation with some added nonlinearities. Self-excited systems, on the other hand, start to oscillate on their own [2]. The vibrations can be reduced in all three cases by improving the system damping. Improving the damping by physical means may not be possible in some applications, such as flexible appendages of a spacecraft.

S. M. Dhobale · S. Chatterjee (✉)
Department of Mechanical Engineering, Indian Institute of Engineering Science and Technology, Shibpur, P.O. Botanic Garden, Howrah, West Bengal 711103, India
e-mail: shychat@gmail.com;
shy.mech@faculty.iiests.ac.in

The simplest way of improving damping by active means is by using direct velocity feedback [3]. Oueini et al. proposed a cubic velocity feedback control to suppress the vibrations in an axially excited cantilever beam [4]. Huang et al. studied the performance of cubic velocity and cubic displacement feedback control in suppressing the vibrations of a parametrically excited system [5]. Tehrani et al. studied the performance of velocity and displacement feedback for controlling parametrically excited systems [6]. Similar studies have been performed for negative velocity feedback with linear [7] and nonlinear control laws [8]. Maccari implemented time-delayed state feedback to control principal parametric resonance [9]. Zhao et al. used delayed position feedback for the vibration suppression of 1:2 principal parametric resonance in a system [10]. Chatterjee proposed recursive time-delayed acceleration feedback for controlling principal and 1:3 subharmonic resonance in a nonlinear system [11]. Control schemes with direct feedback are not immune to the noise and may excite the higher modes of the system. To avoid this spillover effect, Fanson and Caughey first proposed a resonant controller using a second-order filter with positive position feedback (PPF) for active vibration control [12]. If the filter frequency is tuned to the system's natural frequency, the filter adds a phase of $-\pi/2$ to the feedback signal (i.e., position). It generates the force in anti-phase with the velocity, resulting in improved damping at resonance. Sim and Lee applied a similar control strategy with acceleration feedback [13]. Mondal and Chatterjee studied the performance of resonant controllers with velocity feedback and time-delayed nonlinear control law for suppressing the vibrations in a self-excited system [14]. The detailed parametric study of a generalized resonant controller with time delay and fractional-order input can be found in [15]. Abdelhafez et al. used a positive position feedback (PPF) controller with delay to control the vibrations of a beam subjected to both self and external excitations [16].

Few researchers have tried a slightly different approach for active vibration control. Warminski et al. studied the performance of nonlinear saturated control (NSC) to mitigate the vibrations of a beam subjected to both self and external excitations [17]. Kamel et al. used a similar strategy to suppress the vibrations of a nonlinear magnetic levitation system [18] and a compressor blade [19], which is excited by both external and parametric excitations.

Researchers have observed that by adding a parametric excitation, the system's vibrations can be amplified or unamplified by controlling the phase and frequency of the parametric excitation [20–23]. Rahn and Mote proposed a method to obtain a control signal from state variables such as displacement and velocity, where a parametric control signal is chosen to be the product of the displacement and velocity $x(t)\dot{x}(t)$ [24]. Senapati et al. employed a similar strategy to design the stiffness-switching condition and to reduce the vibrations [25]. Chechurin et al. used parametric feedback for fast stabilization of the system [26]. In the proposed scheme, $\text{sgn}\left(\frac{d}{dt}(x(t))^2\right)$ is chosen to be a signal, which controls the length of the pendulum. Pumphossel et al., tried a different approach, where the controller is designed such that the control force is proportional to the negative axial velocity of the tip of the beam [27]. The axial velocity of the tip of the beam is found to be proportional to $x(t)\dot{x}(t)$, where $x(t)$ is the lateral displacement. The optimal parametric control law for the vibration control of a system subjected to random excitations is of the form $R\text{sgn}(x(t)\dot{x}(t))$, where R is a constant [28]. Chang et al. considered the parametric control term as a weighted sum of $x^2(t)$, $x(t)\dot{x}(t)$, and $\dot{x}^2(t)$ to control the vibrations of the system subjected to both direct and parametric random excitations [29].

There are mainly two ways to improve the system damping, viz., by adding a control force out of phase with the velocity or by varying the system parameters, of which the first method has been studied in detail using a generalized resonant control [15]. In the present paper, the system damping is improved by varying the system parameter (here, displacement of the base of a cantilever beam). The primary objective of this study is to design a control law such that the resultant force, due to parameter variation, is purely dissipative while vibrating at the resonance. The control law is formulated as a nonlinear function of the state variables of a second-order filter fed back with the measured acceleration signal of the structure.

If the steady-state displacement signal is of form $x = a_1 \sin(\Omega t)$, the types of controller used in [24–29] generate the control signal (u_1), which, after expanded as a Fourier series, possesses a 2Ω component with zero phase, i.e., $u_1 = a_2 \sin(2\Omega t) + (4\Omega, 6\Omega \dots \text{ terms})$. Thus, the force on the system due to parametric excitation is of the form $u_1 x = \frac{a_1 a_2}{2} \cos(\Omega t)$

$+(3\Omega, 5\Omega, \dots)$ terms), of which the first term, depending on the sign of the control gain, is in anti-phase with the velocity, thereby producing a positive damping effect. But, this type of control also introduces higher harmonics that might not be necessary, and hence the energy spilled in the higher harmonics is not utilized. In this paper, the control law is designed such that the higher harmonics have low energy density compared to the first harmonic term of the control force, u_1x .

2 Mathematical model

A cantilever beam with a bluff body of mass m at the tip is considered as a vibrating system. The base of the beam can move in both transverse and axial directions, as shown in Fig. 1. The beam can be excited due to the axial motion of the base, the transverse motion of the beam and/or due to the air flowing over the bluff body. The non-dimensional equation of motion of a cantilever beam vibrating around the first mode and actively controlled by the parametric feedback is given as (see ‘‘Appendix A’’ for detailed derivation)

$$(1 + \gamma_1x^2)\ddot{x} + (\zeta_1 + \zeta_2x^2)\dot{x} + (1 + \gamma_1x^2)x + \gamma_3x^3 = \lambda_2(F_2 + u_1)x + F_1, \tag{1a}$$

where $\gamma_i (i = 1, 2, 3)$ are nonlinearity parameters that depend on the mode shape function of the beam and ζ_i denote the non-dimensional damping parameters. F_1 and F_2 are the excitation forces comprising direct and parametric terms, respectively. The direct excitation

F_1 comprises harmonic, superharmonic and subharmonic terms. The parametric excitation F_2 consists of principal and superharmonic terms. Thus,

$$F_1 = f_1 \cos(\Omega t + \phi_1) + f_3 \cos(3\Omega t + \phi_3) + f_{1/3} \cos\left(\frac{\Omega}{3}t + \phi_{1/3}\right) \tag{1b}$$

$$F_2 = f_2 \cos(2\Omega t) + f_4 \cos(4\Omega t + \phi_4) \tag{1c}$$

The flow-induced self-excited vibrations can be studied by selecting negative linear damping, i.e. $\zeta_1 < 0$ and positive nonlinear damping, i.e. $\zeta_2 > 0$.

The control input is considered to be a function of the state variables of a resonant filter

$$u_1 = g(z, \dot{z}), \tag{1d}$$

where z is the state variable of a second-order filter fed back with the measured acceleration signal of the structure, i.e.,

$$\ddot{z} + 2\zeta_f\Omega_f\dot{z} + \Omega_f^2z = \ddot{x}. \tag{1e}$$

There are two distinct advantages of using the filter. First, it attenuates the high-frequency noise of the measured signal. Second, the filter frequency can be tuned appropriately to the target mode in an MDOF system.

2.1 Design of the controller

The primary objective here is to design the control input, i.e. the function $g(z, \dot{z})$ such that the control force is purely dissipative. So, the control input, $g(z, \dot{z})$

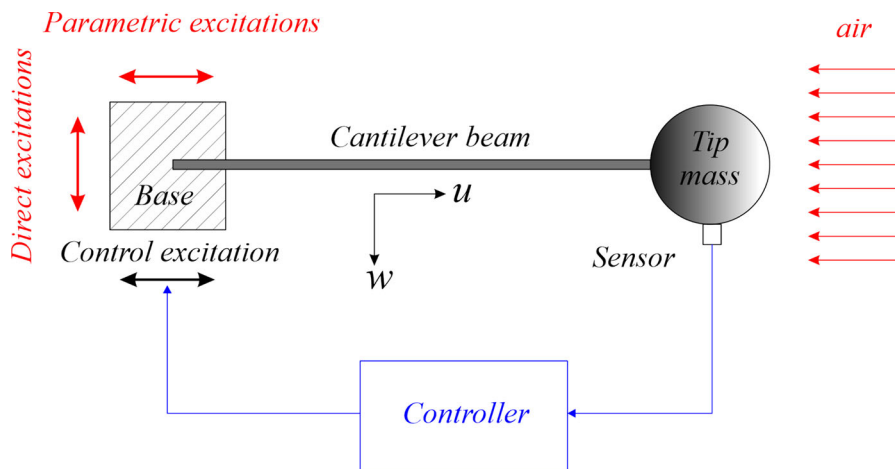
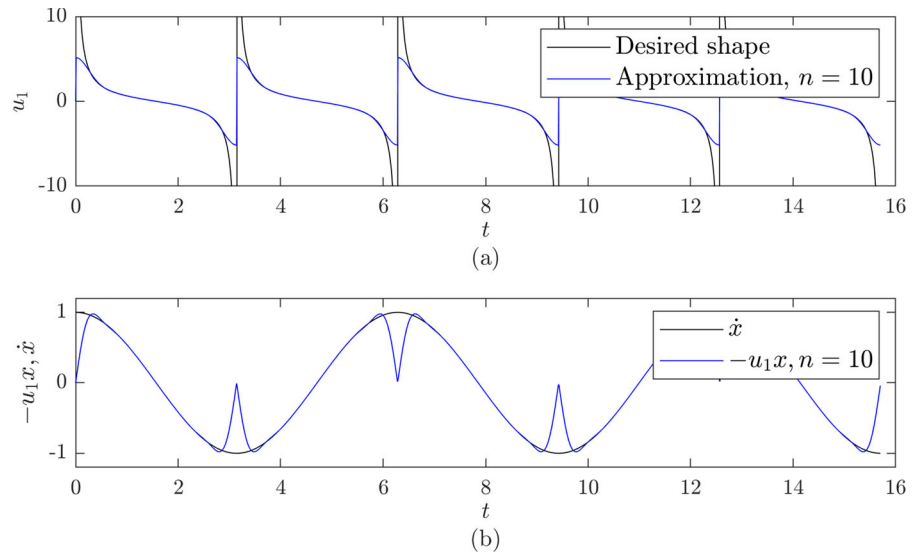


Fig. 1 A schematic model of a cantilever beam vibrating due to direct, parametric, and self-excitations

Fig. 2 a Exact and approximate control signal. **b** Comparison between $-ux$ and velocity signal



should be chosen so that the phase difference between the dominant harmonic component of the control force $\lambda_2 u_1 x$ maintains a 180° phase difference with the velocity, i.e. $-\lambda_2 u_1 x$ is in phase with the velocity.

Let the system response, at the steady state, be dominated by a single frequency and, thus, can be approximated as $x = a \sin(\Omega t + \alpha)$. Therefore, the desired function $g(z, \dot{z})$ must be of the form,

$$u_1 = g(z, \dot{z}) = \cot(\Omega t + \alpha) \tag{1f}$$

Now, if the filter frequency Ω_f is tuned to Ω , the state variables of the filter equation are of the form, $z = b \cos(\Omega t + \alpha)$ and $\dot{z} = -b\Omega \sin(\Omega t + \alpha)$. Thus, the objective has been simplified to generate a *cotangent* curve using *sine* and *cosine* curves. One can use the Fourier series expansion to generate the approximate *cotangent* signal, but it is difficult to generate the high-frequency components separately using only the state variables of the filter. In this paper, the following approximation is used

$$u_1 = k \sum_{i=1}^n c_i (\cos(\Omega t + \alpha))^{2i-1} \text{sgn}(\sin(\Omega t + \alpha)), \tag{2a}$$

where the coefficients c_i 's are obtained by using the least square algorithm to minimize the error between the approximate polynomial and the desired shape of the signal. (Detailed explanation is given in “Appendix C”). The desired and approximate shape of the control signal is shown in Fig. 2a. From Fig. 2b, one observes that the term $-ux$ is almost everywhere in

phase with the velocity, except at some time instances, particularly near the maximum velocity. However, the interval of mismatch can be reduced by increasing the order of approximation n .

But the above approximation requires the *cosine* signal of unit amplitude. To obtain the signal with zero phase shift and unit amplitude from the filter variable z , the following equations are proposed (details are given in “Appendix D”),

$$y = k_{11}z \tag{2b}$$

$$\frac{dk_{11}}{dt} = k_a \left(\frac{1}{2} - (k_{11}z)^2 \right) \tag{2c}$$

Therefore, the system given in Eq. (1) with the proposed controller can be written as

$$\begin{aligned} (1 + \gamma_1 x^2)\ddot{x} + (\zeta_1 + \zeta_2 x^2)\dot{x} + (1 + \gamma_1 x^2)x + \gamma_3 x^3 \\ = \lambda_2 (F_2 + k u_1)x + F_1 \end{aligned} \tag{3a}$$

$$\ddot{z} + 2\zeta_f \Omega_f \dot{z} + \Omega_f^2 z = \ddot{x} \tag{3b}$$

$$\frac{dk_{11}}{dt} = k_a \left(\frac{1}{2} - (k_{11}z)^2 \right) \tag{3c}$$

$$y = k_{11}z \tag{3d}$$

$$u_1 = \sum_{i=1}^n c_i y^{2i-1} \text{sgn}(\dot{z}) \tag{3e}$$

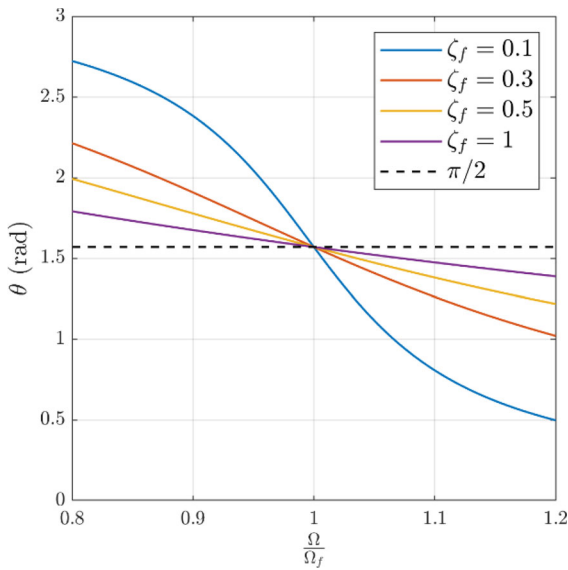


Fig. 3 Effect of filter damping on the sensitivity of the filter phase

While designing the control law, Ω_f was assumed to be tuned to Ω . In the case of resonance, the system vibrates at a frequency close to the natural frequency, i.e. $\Omega \sim 1$. The sensitivity of the phase due to the filter at $\Omega_f = \Omega$ can be controlled by varying the filter damping, as shown in Fig. 3. For the controller to work as expected, higher values of filter damping can be selected to maintain the phase due to the filter being as close as possible to $\pi/2$ for a wide range of frequencies.

3 Nonlinear analysis

In this section, the method of multiple time scales [30] is employed to obtain the approximate system response. Towards this end, Eqs. (3a) and (3b) are recast as,

$$\ddot{x} + \Omega^2 x = \varepsilon(\sigma_1 x - \bar{\gamma}_1 x^2 \ddot{x} - (\bar{\zeta}_1 + \bar{\zeta}_2 x^2) \dot{x} - \bar{\gamma}_3 x^3 - \bar{\gamma}_1 x^2 \dot{x} + u_1 \bar{\lambda}_2 x + F_w) + F_s, \tag{4a}$$

where F_s and F_w are strong and weak excitations,

$$F_s = \frac{f_3}{2} \exp(i3\Omega t + i\phi_3) + \frac{f_{1/3}}{2} \exp\left(i\frac{\Omega}{3} t + i\phi_{1/3}\right) \tag{4b}$$

$$F_w = \left(\frac{f_2}{2} \exp(i2\Omega t) + \frac{f_4}{2} \exp(i4\Omega t + i\phi_4) + cc\right) \bar{\lambda}_2 x + \left(\frac{\bar{f}_1}{2} \exp(i\Omega t + i\phi_1) + cc\right) \tag{4c}$$

$$\ddot{z} + \Omega^2 z = \varepsilon(\sigma_2 z - 2\bar{\zeta}_f \Omega_f \dot{z} + \bar{\varepsilon} \ddot{x}), \tag{4d}$$

and

$$\frac{dk_{11}}{dt} = \varepsilon\left(\bar{k}_a \left(\frac{1}{2} - (k_{11} z)^2\right)\right) \tag{4e}$$

where $\zeta_i = \varepsilon \bar{\zeta}_i$, $\gamma_i = \varepsilon \bar{\gamma}_i$, $\lambda_2 = \varepsilon \bar{\lambda}_2$, $\varepsilon \sigma_1 = \Omega^2 - 1$, $\varepsilon \bar{\zeta}_f = \zeta_f$, $\varepsilon \bar{\varepsilon} = 1$, $\varepsilon \sigma_2 = \Omega^2 - \Omega_f^2$ and $\varepsilon \bar{k}_a = k_a$ with ε as a small parameter. Let, $\tau = t$ and $T = \varepsilon t$ be two-time scales. Thus, the solutions of Eqs. (4a), (4d) and (4e) can be expressed as.

$$x = x_0(\tau, T) + \varepsilon x_1(\tau, T) + O(\varepsilon^2) \tag{5a}$$

$$z = z_0(\tau, T) + \varepsilon z_1(\tau, T) + O(\varepsilon^2) \tag{5b}$$

$$k_{11} = k_{110}(\tau, T) + \varepsilon k_{111}(\tau, T) + O(\varepsilon^2) \tag{5c}$$

It is assumed that the k_a is chosen to be a small value such that the variation of the parameter k_{11} is slow. Therefore it can be assumed that $k_{11} = k_{11}(T)$. Equation (5c) can be rewritten as

$$k_{11} = k_{110}(T) + \varepsilon k_{111}(T) + O(\varepsilon^2) \tag{5d}$$

Substituting the Eqs. (5a), (5b) in Eqs. (4a), (4b) and equating the coefficients of ε^0 , yields

$$D_\tau^2 x_0 + \Omega^2 x_0 = \frac{f_3}{2} \exp(i3\Omega t + i\phi_3) + \frac{f_{1/3}}{2} \exp\left(i\frac{\Omega}{3} t + i\phi_{1/3}\right) + cc \tag{6a}$$

$$D_\tau^2 z_0 + \Omega^2 z_0 = 0 \tag{6b}$$

Solutions of Eqs. (6a) and (6b) are written, respectively as

$$x_0 = \frac{a_{1,1}}{2} \exp(i\Omega \tau + i\alpha_1) + \frac{a_{1,3}}{2} \exp(i3\Omega \tau + i\phi_3) + \frac{a_{1,1/3}}{2} \exp\left(i\frac{\Omega}{3} \tau + i\phi_{1/3}\right) + cc \tag{7a}$$

$$a_{1,3} = -\frac{f_3}{8\Omega^2} \tag{7b}$$

$$a_{1,1/3} = \frac{9f_{1/3}}{8\Omega^2} \tag{7c}$$

$$z_0 = \frac{a_{2,1}}{2} \exp(i\Omega\tau + i\alpha_2) + cc \tag{7d}$$

where $a_{1,1}, a_{2,1}, \alpha_1, \alpha_2$ are functions of T .

Substituting the Eqs. (5d) and (5b) in Eqs. (4e) and equating the coefficients of ϵ^1 , yields

$$\frac{\partial k_{110}}{\partial T} = \bar{k}_a \left(\frac{1}{2} - (k_{11}z_0)^2 \right) \tag{7e}$$

Substituting Eq. (7d) in (7e) and averaging over a period of $\frac{2\pi}{\Omega}$ one obtains

At the steady state, Eq. (7f) yields $k_{11}a_2 = 1$, i.e., the amplitude of the signal y used in Eq. (3c) is unity.

Hence, one can write $y = \cos(\Omega\tau + \alpha_2)$. Now, employing the Fourier series approximation, the following expression is obtained

$$\begin{aligned} \sum_{i=1}^n c_i y^{2i-1} \text{sgn}(\dot{z}) x_0 &\approx c_0 a_{1,1} \cos(\Omega t + 2\alpha_2 - \alpha_1) \\ &= \frac{c_0 a_{1,1}}{2} (\exp(i(\Omega t + 2\alpha_2 - \alpha_1)) + cc) \end{aligned} \tag{7g}$$

Substituting Eqs. (7a–d,g) in Eq. (4a–b), eliminating the secular terms and separating the real and imaginary terms, one obtains the following slow-flow equations

$$\epsilon a'_{1,1} = -\frac{1}{2\Omega} \left(\begin{aligned} &\left(\frac{f_1}{2} \sin(\alpha_1 - \phi_1) \right) + \frac{1}{8} (a_{1,1}^3 \Omega \zeta_2 - a_{1,1/3}^3 \gamma_3 \sin(\alpha_1 - 3\phi_{1/3})) + \frac{1}{24} a_{1,1/3}^3 \Omega \zeta_2 \cos(\alpha_1 - 3\phi_{1/3}) \\ &+ \frac{1}{4} a_{1,3} f_4 \lambda_2 \sin(\alpha_1 + \phi_3 - \phi_4) - \frac{3}{8} a_{1,1}^2 a_{1,3} \gamma_3 \sin(3\alpha_1 - \phi_3) + \frac{1}{36} a_{1,1/3}^3 \gamma_1 \Omega^2 \sin(\alpha_1 - 3\phi_{1/3}) \\ &+ \frac{1}{4} a_{1,1} a_{1,3}^2 \Omega \zeta_2 + \frac{1}{4} a_{1,1} a_{1,1/3}^2 \Omega \zeta_2 + \frac{1}{4} a_{1,3} f_2 \lambda_2 \sin(\alpha_1 - \phi_3) + \frac{1}{4} a_{1,1} f_2 \lambda_2 \sin(2\alpha_1) + \frac{1}{2} a_{1,1} \Omega \zeta_1 \\ &+ \frac{3}{4} a_{1,1}^2 a_{1,3} \gamma_1 \Omega^2 \sin(3\alpha_1 - \phi_3) - \frac{1}{2} a_{1,1} c_0 k \lambda_2 \cos(2\alpha_1 - 2\alpha_2) + \frac{1}{8} a_{1,1}^2 a_{1,3} \Omega \zeta_2 \cos(3\alpha_1 - \phi_3) \end{aligned} \right) \tag{8a}$$

$$\epsilon \alpha'_1 = -\frac{1}{2a_{1,1}\Omega} \left(\begin{aligned} &\left(\frac{1}{2} a_{1,1} \Omega^2 - \frac{3}{8} a_{1,1}^3 \gamma_3 - \frac{1}{2} a_{1,1} + \frac{1}{2} f_1 \cos(\alpha_1 - \phi_1) + \frac{1}{4} a_{1,1}^3 \gamma_1 \Omega^2 - \frac{1}{8} a_{1,1/3}^3 \gamma_3 \cos(\alpha_1 - 3\phi_{1/3}) \right. \\ &- \frac{3}{4} a_{1,1} a_{1,3}^2 \gamma_3 - \frac{3}{4} a_{1,1} a_{1,1/3}^2 \gamma_3 - \frac{1}{24} a_{1,1/3}^3 \Omega \zeta_2 \sin(\alpha_1 - 3\phi_{1/3}) - \frac{3}{8} a_{1,1}^2 a_{1,3} \gamma_3 \cos(3\alpha_1 - \phi_3) \\ &+ \frac{1}{36} a_{1,1/3}^3 \gamma_1 \Omega^2 \cos(\alpha_1 - 3\phi_{1/3}) + \frac{1}{4} a_{1,3} f_2 \lambda_2 \cos(\alpha_1 - \phi_3) + \frac{1}{4} a_{1,1} f_2 \lambda_2 \cos(2\alpha_1) \\ &+ \frac{5}{2} a_{1,1} a_{1,3}^2 \gamma_1 \Omega^2 + \frac{5}{18} a_{1,1} a_{1,1/3}^2 \gamma_1 \Omega^2 + \frac{1}{4} a_{1,3} f_4 \lambda_2 \cos(\alpha_1 + \phi_3 - \phi_4) \\ &\left. + \frac{3}{4} a_{1,1}^2 a_{1,3} \gamma_1 \Omega^2 \cos(3\alpha_1 - \phi_3) + \frac{1}{2} a_{1,1} c_0 k \lambda_2 \sin(2\alpha_1 - 2\alpha_2) - \frac{1}{8} a_{1,1}^2 a_{1,3} \Omega \zeta_2 \sin(3\alpha_1 - \phi_3) \right) \end{aligned} \right) \tag{8b}$$

$$\frac{\partial k_{110}}{\partial T} = \frac{\bar{k}_a}{2} (1 - k_{11}^2 a_{21}^2) \tag{7f}$$

$$\epsilon a'_{2,1} = -\frac{1}{2\Omega} \left(a_{2,1} \Omega \Omega_f \zeta_f + \frac{1}{2} a_{1,1} \Omega^2 \sin(\alpha_1 - \alpha_2) \right) \tag{8c}$$

$$\varepsilon \alpha'_{2,1} = \frac{1}{4a_{2,1}\Omega} \left(a_{2,1} (\Omega_f^2 - \Omega^2) + a_{1,1} \Omega^2 \cos(\alpha_1 - \alpha_2) \right) \tag{8d}$$

Applying the steady-state conditions i.e., $a'_1 = a'_2 = \alpha'_1 = \alpha'_2 = 0$ in Eqs. (8a–d) yields

$$A_j(a_i, \alpha_i) = 0, \tag{8e}$$

for $j = 1, \dots, 4$ and $i = 1, 2$

Solving Eqs. (8e), one obtains the steady-state response of the system. The stability of the steady-state solutions is determined by the eigenvalues of the Jacobian (J) of the slow-flow Eqs. (8a–d).

$$J = \begin{bmatrix} \frac{\partial a'_{1,1}}{\partial a_{1,1}} & \frac{\partial a'_{1,1}}{\partial \alpha_1} & \frac{\partial a'_{1,1}}{\partial a_{2,1}} & \frac{\partial a'_{1,1}}{\partial \alpha_2} \\ \frac{\partial \alpha'_{2,1}}{\partial a_{1,1}} & \frac{\partial \alpha'_{2,1}}{\partial \alpha_1} & \frac{\partial \alpha'_{2,1}}{\partial a_{2,1}} & \frac{\partial \alpha'_{2,1}}{\partial \alpha_2} \\ \frac{\partial a'_{2,1}}{\partial a_{1,1}} & \frac{\partial a'_{2,1}}{\partial \alpha_1} & \frac{\partial a'_{2,1}}{\partial a_{2,1}} & \frac{\partial a'_{2,1}}{\partial \alpha_2} \\ \frac{\partial \alpha'_{1,1}}{\partial a_{1,1}} & \frac{\partial \alpha'_{1,1}}{\partial \alpha_1} & \frac{\partial \alpha'_{1,1}}{\partial a_{2,1}} & \frac{\partial \alpha'_{1,1}}{\partial \alpha_2} \end{bmatrix} \tag{9}$$

4 Numerical results

In this section, different possible nonlinear resonant conditions are considered and the efficacy of the controller is demonstrated for each individual case.

4.1 Principal parametric resonance

$$(f_i = 0, i \neq 2, \zeta_1 > 0)$$

For pure principal parametric excitation, Eq. 8e can be recast as

$$a_{1,1} \left((\zeta_1 \Omega - c_0 k \lambda_2 \cos 2\theta) + \frac{1}{4} \zeta_2 \Omega a_{1,1}^2 \right) = a_{1,1} \left(-\frac{1}{2} f_2 \lambda_2 \sin 2\alpha_1 \right) \tag{10a}$$

$$a_{1,1} \left((1 - \Omega^2 + k c_0 \lambda_2 \sin 2\theta) + \frac{1}{4} (3\gamma_3 - 2\gamma_1 \Omega^2) a_{1,1}^2 \right) = a_{1,1} \left(\frac{1}{2} f_2 \lambda_2 \cos 2\alpha_1 \right) \tag{10b}$$

$$a_{2,1} = \frac{a_{1,1} \Omega^2}{\sqrt{(\Omega_f^2 - \Omega^2)^2 + (2\zeta_f \Omega_f \Omega)^2}} \tag{10c}$$

$$\alpha_2 - \alpha_1 = \theta = \tan^{-1} \left(\frac{2\zeta_f \Omega_f \Omega}{\Omega^2 - \Omega_f^2} \right) \tag{10d}$$

Simplifying the Eqs. (10a–10d), one obtains a polynomial equation

$$(d_2 a_{1,1}^4 + d_1 a_{1,1}^2 + d_0) a_{1,1}^2 = 0, \tag{11a}$$

$$d_2 a_{1,1}^4 + d_1 a_{1,1}^2 + d_0 = 0 \tag{11b}$$

where

$$d_2 = \frac{1}{16} \left((\zeta_2 \Omega)^2 + (2\gamma_1 \Omega^2 - 3\gamma_3)^2 \right)$$

$$d_1 = \frac{1}{2} \left((\zeta_1 \Omega - k \lambda_2 c_0 \cos 2\theta) \zeta_2 \Omega - (2\gamma_1 \Omega^2 - 3\gamma_3) (1 - \Omega^2 + k \lambda_2 c_0 \sin 2\theta) \right)$$

$$d_0 = (\zeta_1 \Omega)^2 + (\Omega^2 - 1)^2 - 2k \lambda_2 c_0 \left((\Omega^2 - 1) \sin 2\theta + \zeta_1 \Omega \cos 2\theta \right) + (k \lambda_2 c_0)^2 - \left(\frac{f_2 \lambda_2}{2} \right)^2$$

Solving Eq. (11b), one obtains the amplitude of the system response $a_{1,1}$ for the chosen control parameters and oscillation frequency Ω . Other unknowns, such as $a_{2,1}$, α_1 and α_2 can be obtained from Eqs. (10a-10d). It can be observed that Eq. (11a) possess a trivial solution $a_{1,1} = 0$ indicating the static equilibrium as one of the steady-state solutions of the system.

Equation (11b) may have either 0, 1, or 2 real roots depending on the parameter values. Thus, a value of the control gain exists, k beyond which Eq. (11b) does not have a real root implying complete suppression of vibration (i.e., stable static equilibrium). To ensure the nonexistence of any real root, the coefficients of the polynomial (11b) must satisfy one of the following criteria.

Case I: $d_1^2 - 4d_0d_2 < 0$.

Case II: $d_1 > 0$ and $d_0 > 0$.

Figure 4a depicts the regions of the number of roots of the polynomial (11) in k versus Ω plane. It can be observed that there exists a minimum value of k above which there exists no real solution, and hence complete suppression of vibration can be achieved.

Figure 4b illustrates the analytical frequency response plot (obtained from Eq. (11)). The analytical results are verified by the numerical simulations.

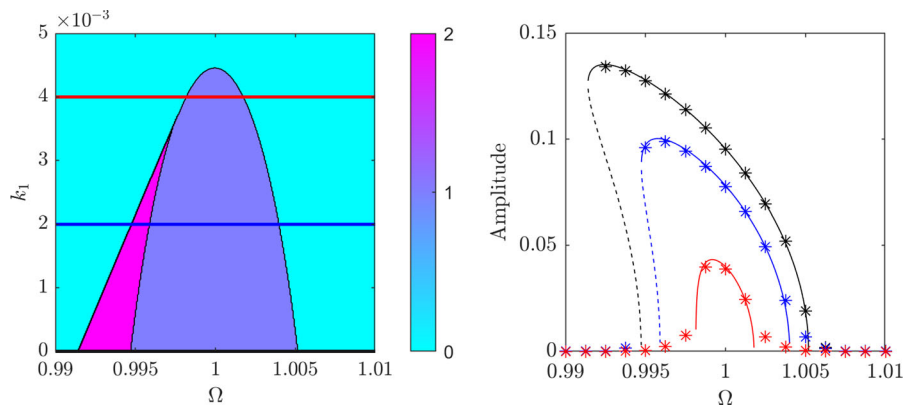


Fig. 4 Effect of control gain on the frequency response of the system $k = 0$ (black), $k = 0.002$ (blue), $k = 0.004$ (red). $\zeta_1 = 0.01$, $\zeta_2 = 1$, $\gamma_1 = 2.9053$, $\gamma_3 = 0.8174$, $\lambda_2 = 1.1575$, $f_2 = 0.025$, $k_a = 1$, $\zeta_f = 1$, $\Omega_f = 1$, $n = 10$

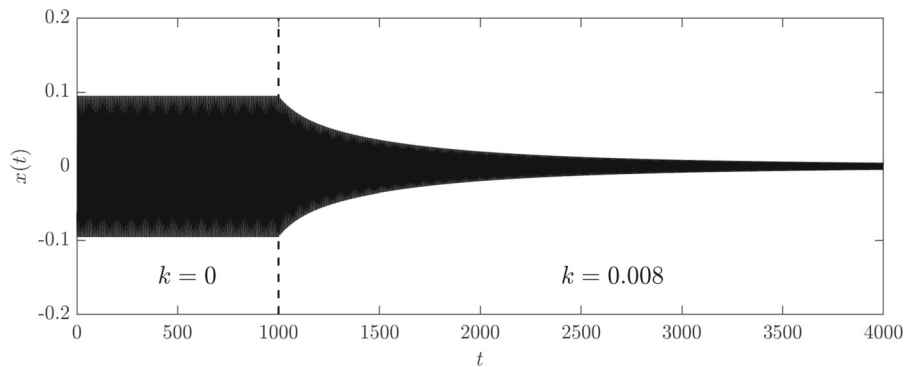


Fig. 5 Time history plot of the uncontrolled and controlled system response (Simulation) $\zeta_1 = 0.01$, $\zeta_2 = 1$, $\gamma_1 = 2.9053$, $\gamma_3 = 0.8174$, $\lambda_2 = 1.1575$, $f_2 = 0.025$, $k_a = 2$, $\zeta_f = 1$, $\Omega_f = 1$, $n = 10$

At $\Omega = 1$ and $\Omega_f = 1$, the expression $d_0 > 0$ yields the following threshold value of the control gain above which the parametric resonance is completely suppressed

$$k > \frac{-\zeta_1 + \frac{f_2 \lambda_2}{2}}{\lambda_2 c_0} \tag{12}$$

For an uncontrolled system, the threshold value of parametric excitation amplitude above which the parametric resonance can be observed is obtained as

$$(f_2)_{critical} = \frac{2\zeta_1}{\lambda_2} \tag{13}$$

Thus, the threshold value of the control gain, k given by Eq. (12), is valid provided $f_2 > (f_2)_{critical}$, i.e., the control gain must be positive ($k > 0$).

Figure 5 shows the system response time-history plot for uncontrolled and controlled cases.

4.2 Direct excitation

4.2.1 Primary resonance ($f_i = 0, i \neq 1, \zeta_1 > 0$)

For pure primary resonance, one recasts Eq. (8e) as

$$(\zeta_1 \Omega - k_1 \lambda_2 c_0 \cos 2\theta) a_{1,1} + \frac{1}{4} \zeta_2 \Omega a_{1,1}^3 = f_1 \sin(\phi - \alpha_1) \tag{14a}$$

$$(k_1 \lambda_2 c_0 \sin(2\alpha_2 - 2\alpha_1) + 1 - \Omega^2) a_{1,1} - \left(\frac{2}{4} \gamma_1 \Omega^2 - \frac{3}{4} \gamma_3\right) a_{1,1}^3 = f_1 \cos(\phi - \alpha_1) \tag{14b}$$

$$a_{2,1} = \frac{a_{1,1} \Omega^2}{\sqrt{(\Omega_f^2 - \Omega^2)^2 + (2\zeta_f \Omega_f \Omega)^2}} \tag{14c}$$

$$\alpha_2 - \alpha_1 = \theta = \tan^{-1} \left(\frac{2\zeta_f \Omega_f \Omega}{\Omega^2 - \Omega_f^2} \right) \tag{14d}$$

Simplifying Eqs. (14a-d), yields the following polynomial equation

$$e_3 y^3 + e_2 y^2 + e_1 y + e_0 = 0, \tag{15}$$

where

$$e_3 = \frac{1}{16} \left((\zeta_2 \Omega)^2 + (2\gamma_1 \Omega^2 - 3\gamma_3)^2 \right)$$

$$e_2 = \left(\frac{1}{2} \zeta_2 \Omega \right) (\zeta_1 \Omega - k_1 \lambda_2 c_0 \cos(2\alpha_2 - 2\alpha_1)) - \left(\gamma_1 \Omega^2 - \frac{3}{2} \gamma_3 \right) (k_1 \lambda_2 c_0 \sin(2\alpha_2 - 2\alpha_1) + 1 - \Omega^2)$$

$$e_1 = (k_1 \lambda_2 c_0 \sin(2\alpha_2 - 2\alpha_1) + 1 - \Omega^2)^2 + (\zeta_1 \Omega - k_1 \lambda_2 c_0 \cos(2\alpha_2 - 2\alpha_1))^2$$

$$e_0 = -f_1^2$$

and $y = a_{1,1}^2$.

Analytical frequency response plots obtained from Eq. (15) are shown in Fig. 6 for different gain values, k and the results are verified by numerical simulations. Clearly, the proposed controller can significantly

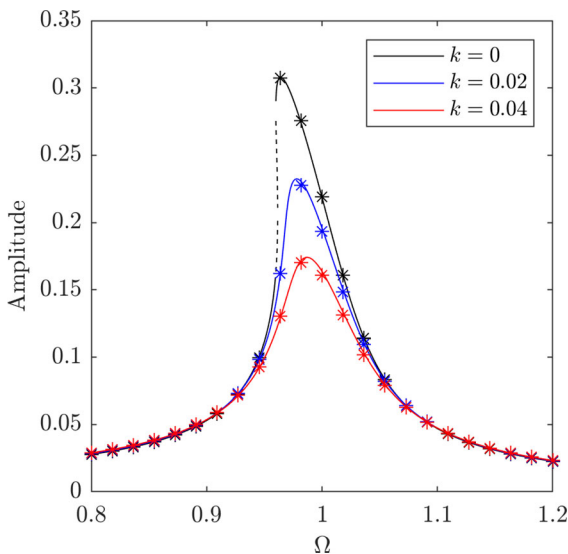


Fig. 6 Effect of gain on the frequency response plots of the system subjected to direct excitation. $\zeta_1 = 0.01$, $\zeta_2 = 1$, $\gamma_1 = 2.9053$, $\gamma_3 = 0.8174$, $\lambda_2 = 1.1575$, $f_2 = 0$, $k_a = 2$, $\zeta_f = 1$, $\Omega_f = 1$, $n = 10$

reduce the resonant vibrations of a directly excited system.

4.2.2 1/3 Subharmonic resonance

($f_i = 0, i \neq 1/3, \zeta_1 > 0$)

For this case, Eq. (8e) yields

$$\begin{aligned} & \frac{1}{4} \zeta_2 \Omega a_{1,1}^2 + \left(\frac{1}{2} \zeta_2 \Omega a_{1,3}^2 + \zeta_1 \Omega - c_0 k \lambda_2 \cos 2\theta \right) \\ & = -\frac{1}{4} a_{1,1} a_{1,3} \Omega \zeta_2 \cos(3\alpha_1 - \phi_3) \\ & + \frac{3}{4} (\gamma_3 - 2\gamma_1 \Omega^2) a_{1,1} a_{1,3} \sin(3\alpha_1 - \phi_3) \end{aligned} \tag{16a}$$

$$\begin{aligned} & \frac{3}{4} (-\gamma_3 + 2\gamma_1 \Omega^2) a_{1,1}^2 + \left((\Omega^2 - 1) - \frac{3}{2} a_{1,3}^2 \gamma_3 + \frac{5}{2} a_{1,3}^2 \gamma_1 \Omega^2 - c_0 k \lambda_2 \sin 2\theta \right) \\ & = \frac{3}{4} (\gamma_3 - 2\gamma_1 \Omega^2) a_{1,1} a_{1,3} \cos(3\alpha_1 - \phi_3) + \frac{1}{4} a_{1,1} a_{1,3} \Omega \zeta_2 \sin(3\alpha_1 - \phi_3) \end{aligned} \tag{16b}$$

$$a_{2,1} = \frac{a_{1,1} \Omega^2}{\sqrt{(\Omega_f^2 - \Omega^2)^2 + (2\zeta_f \Omega_f \Omega)^2}} \tag{16c}$$

$$\alpha_2 - \alpha_1 = \theta = \tan^{-1} \left(\frac{2\zeta_f \Omega_f \Omega}{\Omega^2 - \Omega_f^2} \right) \tag{16d}$$

Simplifying the Eqs. (14a-d), a quadratic equation is obtained as follows:

$$g_2 y^2 + g_1 y + g_0 = 0, \tag{17}$$

where

$$g_2 = \left(\frac{1}{4} \zeta_2 \Omega \right)^2 + \left(\frac{3}{4} (-\gamma_3 + 2\gamma_1 \Omega^2) \right)^2,$$

$$\begin{aligned} g_1 = & 2 \left(\frac{1}{4} \zeta_2 \Omega \right) \left(\frac{1}{2} \zeta_2 \Omega a_{1,3}^2 + \zeta_1 \Omega - c_0 k \lambda_2 \cos 2\theta \right) \\ & - \left(\frac{3}{4} (\gamma_3 - 2\gamma_1 \Omega^2) a_{1,3} \right)^2 - \left(\frac{1}{4} a_{1,3} \Omega \zeta_2 \right)^2 + \frac{3}{2} (-\gamma_3 + 2\gamma_1 \Omega^2) \\ & \left((\Omega^2 - 1) - \frac{3}{2} a_{1,3}^2 \gamma_3 + \frac{5}{2} a_{1,3}^2 \gamma_1 \Omega^2 - c_0 k \lambda_2 \sin 2\theta \right), \end{aligned}$$

$$\begin{aligned} g_0 = & \left((\Omega^2 - 1) - \frac{3}{2} a_{1,3}^2 \gamma_3 + \frac{5}{2} a_{1,3}^2 \gamma_1 \Omega^2 - c_0 k \lambda_2 \sin 2\theta \right)^2 \\ & + \left(\frac{1}{2} \zeta_2 \Omega a_{1,3}^2 + \zeta_1 \Omega - c_0 k \lambda_2 \cos 2\theta \right)^2 \end{aligned}$$

and $y = a_{1,1}^2$.

Equation (17) possess at least one positive real root if, $g_1 < 0$ and $4g_1g_2 < g_1^2$. Figure 7 shows the region of stable 1/3 subharmonic resonance in f_3 versus Ω plane, where the stability boundaries are defined by the equation $g_1^2 - 4g_0g_2 = 0$. Figure 8 shows the effect of excitation and control gain on the system response. It can be observed that the size of the Isola decreases with the decreasing excitation amplitude, f_3 , and the increasing control gain, k , and vice versa. Thus, it is apparent from Figs. 7 and 8 that the proposed control can completely eliminate subharmonic resonance provided the gain is selected above a critical value.

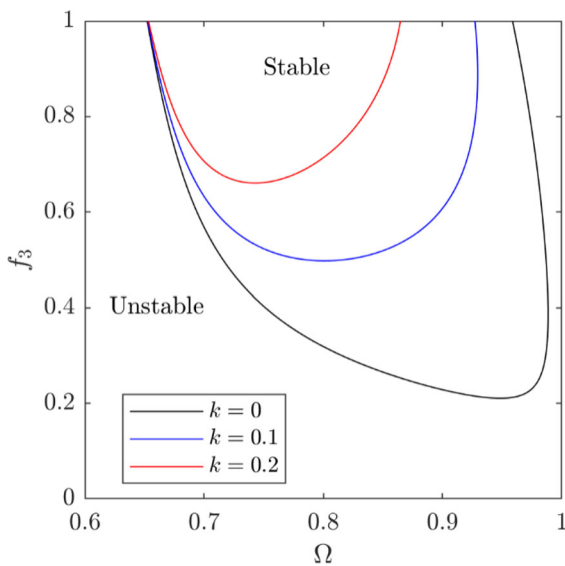
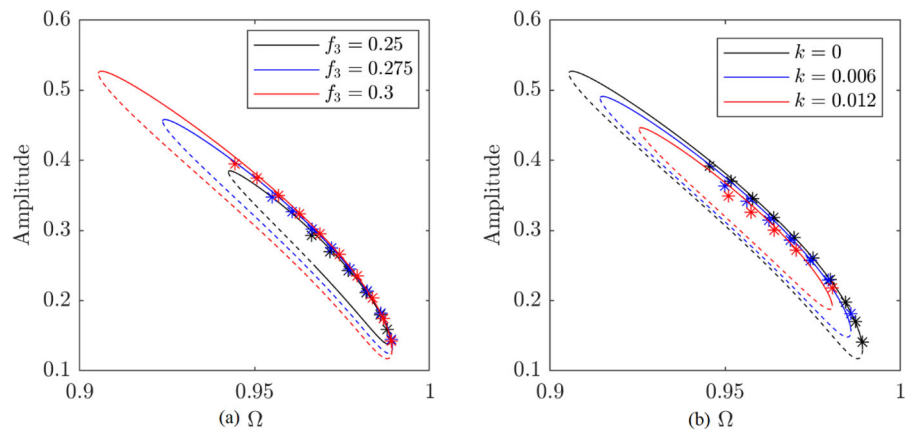


Fig. 7 Effect of gain on the stability region of 1/3 subharmonic resonance

Fig. 8 Effect of **a** excitation amplitude, f_3 , and **b** control gain, k on the amplitude versus frequency curve.

$\zeta_1 = 0.01, \zeta_2 = 1,$
 $\gamma_1 = 2.9053, \gamma_3 = 0.8174,$
 $\lambda_2 = 1.1575, f_2 = 0,$
 $k_a = 30, \zeta_f = 1, \Omega_f = 1,$
 $n = 1$



4.2.3 Simultaneous primary and 1/3 subharmonic resonance ($f_i = 0, i \neq \{1, 3\}, \zeta_1 > 0$)

For this case, Eqs. (8e) yields four nonlinear algebraic equations that cannot be simplified to polynomial form. Hence, the equations are solved using the method of continuation. The results thus obtained are shown in Fig. 9 and verified by numerical simulations. Figure 9a shows the effect of f_3 on the frequency response of a directly excited system. The superharmonic excitation amplifies the system response due to subharmonic resonance. Though the proposed controller is designed for controlling the vibrations with a single frequency, it works effectively in the case of the system vibrating at two frequencies with one dominant frequency, as shown in Fig. 9b.

4.2.4 Simultaneous Primary and 3/1 superharmonic resonance ($f_i = 0, i \neq \{1, 1/3\}, \zeta_1 > 0$)

Equations (8e) is solved, and the effects of the excitation amplitude and the control gain are shown in Fig. 10a, b, respectively. The subharmonic excitation, $f_{1/3}$, tends to amplify the system response due to superharmonic resonance. In this case, the system response consists of two frequency components. Though the control input u is designed for a system dominated by a single frequency close to the natural frequency, the proposed controller can control the system response. Due to the same reason, the mismatch between the analytical and simulation results can be observed in Fig. 10b at lower amplitude levels (where the Ω component is not dominating).

Fig. 9 Effect of **a** excitation amplitude, f_3 and **b** control gain, k , on the frequency response of the system.

$\zeta_1 = 0.01, \zeta_2 = 1,$
 $\gamma_1 = 2.9053, \gamma_3 = 0.8174,$
 $\lambda_2 = 1.1575, f_1 = 0.01,$
 $k_a = 1, \zeta_f = 1, \Omega_f = 1,$
 $n = 1$

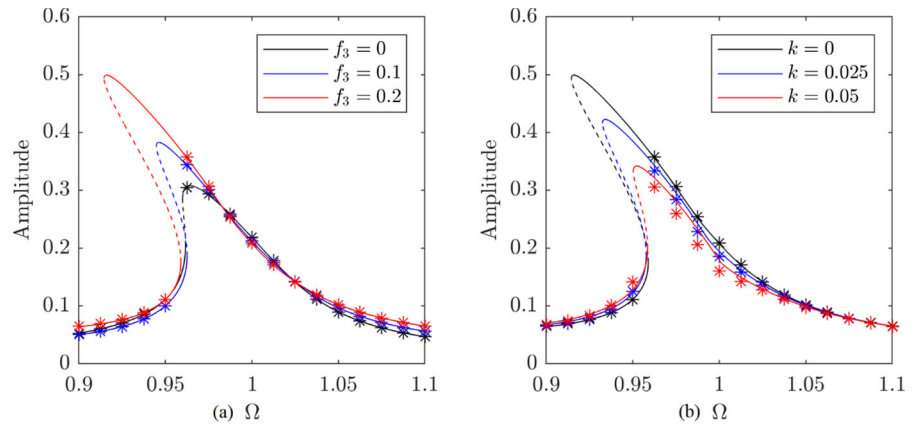
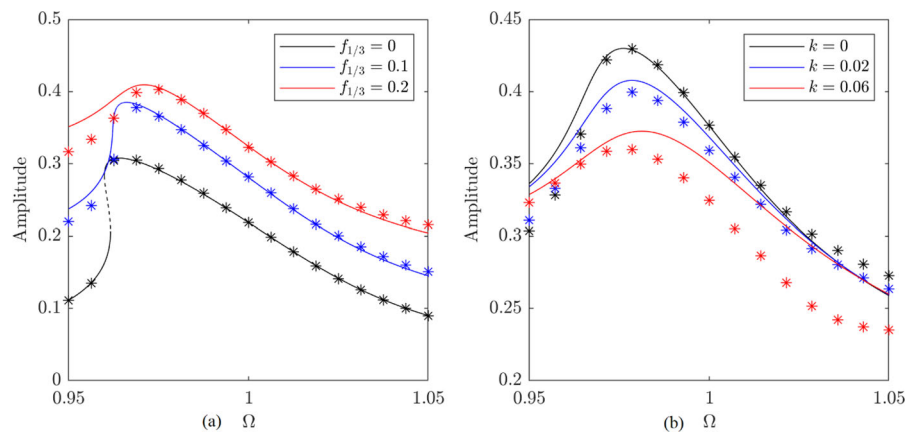


Fig. 10 Effect of **a** 3/1 excitation amplitude $f_{1/3}$, $k = 0$ and, **b** control gain k , $f_{1/3} = 0.2$, on the frequency response of the system.

$\zeta_1 = 0.01, \zeta_2 = 1,$
 $\gamma_1 = 2.9053, \gamma_3 = 0.8174,$
 $\lambda_2 = 1.1575, f_1 = 0.01,$
 $\phi_1 = 0, \phi_{1/3} = 1.5708,$
 $k_a = 1, \zeta_f = 1, \Omega_f = 1,$
 $n = 1$



4.3 Self-excited resonance ($f_i = 0, \zeta_1 < 0$)

In this section, the vibration control of a self-excited system using the proposed controller is investigated. The self-excitation dynamics can be modeled by incorporating negative linear damping ζ_1 and positive nonlinear damping ζ_2 . Substituting the steady state conditions in Eq. (8e) yields

$$a_{2,1} = \frac{a_{1,1}\Omega^2}{\sqrt{(\Omega_f^2 - \Omega^2)^2 + (2\zeta_f\Omega_f\Omega)^2}} \tag{18a}$$

$$\alpha_2 - \alpha_1 = \theta = \tan^{-1}\left(\frac{2\zeta_f\Omega_f\Omega}{\Omega^2 - \Omega_f^2}\right) \tag{18b}$$

$$a_{1,1}^2 = \frac{4(-\zeta_1\Omega + k_1\lambda_2c_0 \cos 2\theta)}{\zeta_2\Omega} \tag{18c}$$

and

$$\sum_{i=0}^7 b_i\Omega^i = 0, \tag{18d}$$

where

$$b_0 = -3c_0\gamma_3k\lambda_2\Omega_f^4$$

$$b_1 = 3\gamma_3\Omega_f^4\zeta_1 - \Omega_f^4\zeta_2$$

$$b_2 = 2c_0\gamma_1k\lambda_2\Omega_f^4 + 4c_0k\lambda_2\zeta_2\Omega_f^3\zeta_f + 12c_0\gamma_3k\lambda_2\Omega_f^2\zeta_f^2 + 6c_0\gamma_3k\lambda_2\Omega_f^2$$

$$b_3 = 2\Omega_f^2\zeta_2 + \Omega_f^4\zeta_2 - 2\gamma_1\Omega_f^4\zeta_1 - 6\gamma_3\Omega_f^2\zeta_1 - 4\Omega_f^2\zeta_2\zeta_f^2 + 12\gamma_3\Omega_f^2\zeta_1\zeta_f^2$$

$$b_4 = -8c_0\gamma_1k\lambda_2\Omega_f^2\zeta_f^2 - 4c_0\gamma_1k\lambda_2\Omega_f^2 - 4c_0k\lambda_2\zeta_2\Omega_f\zeta_f - 3c_0\gamma_3k\lambda_2$$

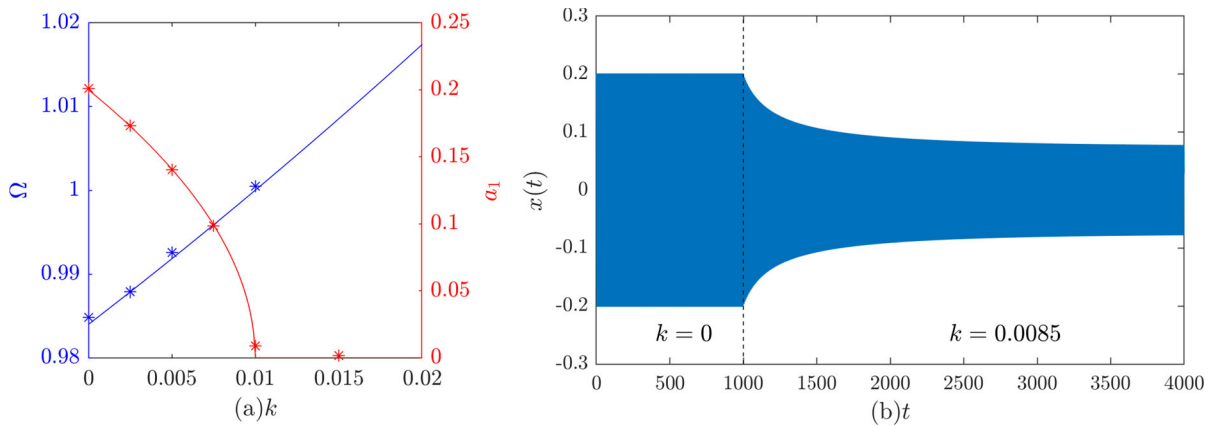
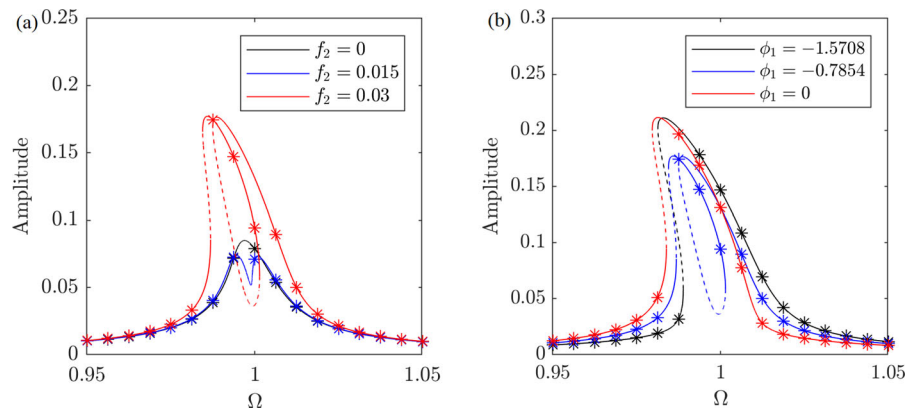


Fig. 11 **a** Variation of frequency and amplitude of a self-excited system with varying gain **b** Simulated response of a self-excited system with and without control. $\zeta_1 = -0.01, \zeta_2 = 1, \gamma_1 = 2.9053, \gamma_3 = 0.8174, \lambda_2 = 1.1575, f_2 = 0, k_a = 1, \zeta_f = 1, \Omega_f = 1, n = 10$

Fig. 12 Effect of **a** Amplitude of parametric excitation and **b** phase of the direct excitation on the frequency response of the uncontrolled system. $\zeta_1 = 0.01, \zeta_2 = 1, f_1 = 0.001, \gamma_1 = 2.9053, \gamma_3 = 0.8174, \lambda_2 = 1.1575$



$$b_5 = 4\Omega_f^2 \zeta_2 \zeta_f^2 + 3\gamma_3 \zeta_1 - 2\Omega_f^2 \zeta_2 + 4\gamma_1 \Omega_f^2 \zeta_1 - \zeta_2 - 8\gamma_1 \Omega_f^2 \zeta_1 \zeta_f^2$$

$$b_6 = 2c_0 \gamma_1 k \lambda_2$$

$$b_7 = \zeta_2 - 2\gamma_1 \zeta_1$$

Solving the Eqs. (18a–d), one obtains the frequency Ω and amplitude a_1 of the system at the steady state. The variations of the frequency and amplitude of oscillations with gain are plotted in Fig. 11a. It can be observed that the self-excited oscillations can be suppressed by selecting the gain above some threshold value, k_{thr} given by

$$k_{thr} = \frac{-\zeta_1}{\lambda_2 c_0} \tag{20}$$

Figure 11b shows the simulated response of the system with and without control.

4.4 Simultaneous direct and parametric resonances

4.4.1 Primary and 1/2 parametric resonance ($f_i = 0, i \neq \{1, 2\}, \zeta_1 > 0$)

Figure 12 shows the frequency response of the system for different amplitudes of parametric excitation, f_2 and phase of the direct excitation, ϕ_1 . It can be observed from Fig. 12a that a loop appears in the frequency response curve when the amplitude of the parametric excitation exceeds the critical value

$(f_2)_{critical} = \frac{2\zeta_1}{\lambda_2}$ (here 0.0173). The existence of the loop also depends on the phase of the direct excitation, ϕ_1 as shown in Fig. 12b

Figure 13 shows the effectiveness of the proposed controller for suppressing the vibrations of the system subjected to both direct and parametric excitations. Evidently, the loop in the frequency response curve disappears beyond a threshold value of the control gain, k (Here, the threshold value of control gain is calculated from Eq. (14) as 0.0073).

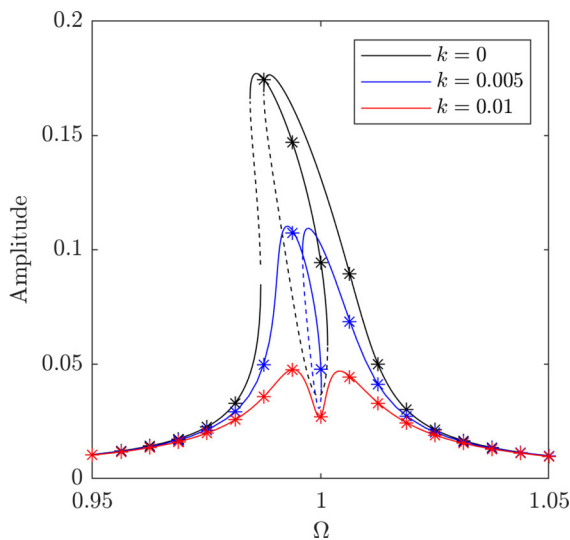
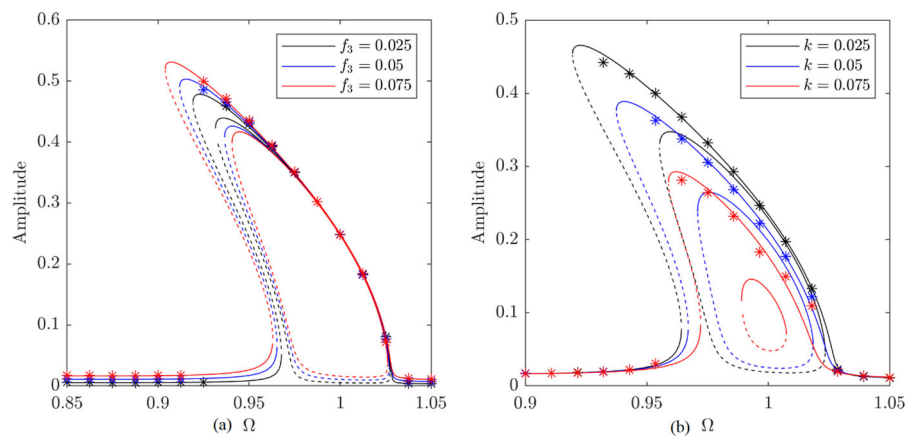


Fig. 13 Effect of control gain on the frequency response of the system. $\zeta_1 = 0.01$, $\zeta_2 = 1$, $\gamma_1 = 2.9053$, $\gamma_3 = 0.8174$, $\lambda_2 = 1.1575$, $f_1 = 0.001$, $\phi_1 = -\pi/4$, $f_2 = 0.03$, $f_3 = 0$, $k_a = 1$, $\zeta_f = 1$, $\Omega_f = 1$, $n = 10$

Fig. 14 Effect of **a** f_3 , $k = 0$ and **b** control gain k , $f_3 = 0.075$ on the frequency response of the system. $f_{1/3} = 0$, $\zeta_1 = 0.01$, $\zeta_2 = 1$, $\gamma_1 = 2.9053$, $\gamma_3 = 0.8174$, $\lambda_2 = 1.1575$, $f_1 = 0$, $f_2 = 0.1$, $f_3 = 0.075$, $f_4 = 0$, $f_{1/3} = 0$, $\phi_1 = 0$, $\phi_3 = 0$, $\phi_4 = 0$, $\phi_{1/3} = 0$, $k_a = 1$, $\zeta_f = 1$, $\Omega_f = 1$, $n = 1$



4.4.2 Simultaneous 1/2 parametric and 1/3 direct subharmonic resonance ($f_i = 0, i \neq \{2, 3\}, \zeta_1 > 0$)

Figure 14a shows the frequency response of the system under simultaneous 1/3-rd subharmonic and 1/2 parametric resonance without control. The formation of isolated resonance is apparent in the frequency response plot. The effectiveness of the control in suppressing the resonance amplitude is evident from Fig. 14b.

4.4.3 Simultaneous 1/2 parametric and 3/1 direct superharmonic resonance ($f_i = 0, i \neq \{2, 1/3\}, \zeta_1 > 0$)

Figure 15 shows the frequency response of the system under simultaneous 3/1 superharmonic and 1/2 parametric resonance with and without control. The effectiveness of the control is evident from these figures.

4.4.4 1/3 Direct and 1/4 parametric subharmonic resonance ($f_i = 0, i \neq \{3, 4\}, \zeta_1 > 0$)

Figure 16 shows the effect of amplitude, f_4 , and phase, ϕ_4 of 4:1 parametric excitation on the system subjected to weak 1:1 direct excitation, f_1 and strong 3:1 direct excitation, f_3 . It can be observed that phase ϕ_4 can either amplify or de-amplify the system response. The proposed controller can suppress the subharmonic resonances and their combinations as shown in Fig. 17.

Fig. 15 Effect of **a** $f_{1/3}$, $k = 0$ and **b** control gain k , $f_{1/3} = 0.08$ on the frequency response of the system. $\zeta_1 = 0.01, \zeta_2 = 1, \gamma_1 = 2.9053, \gamma_3 = 0.8174, \lambda_2 = 1.1575, f_1 = 0, f_2 = 0.1, f_3 = 0, f_4 = 0, \phi_1 = 0, \phi_3 = 0, \phi_4 = 0, \phi_{1/3} = 0, k_a = 1, \zeta_f = 1, \Omega_f = 1, n = 1$

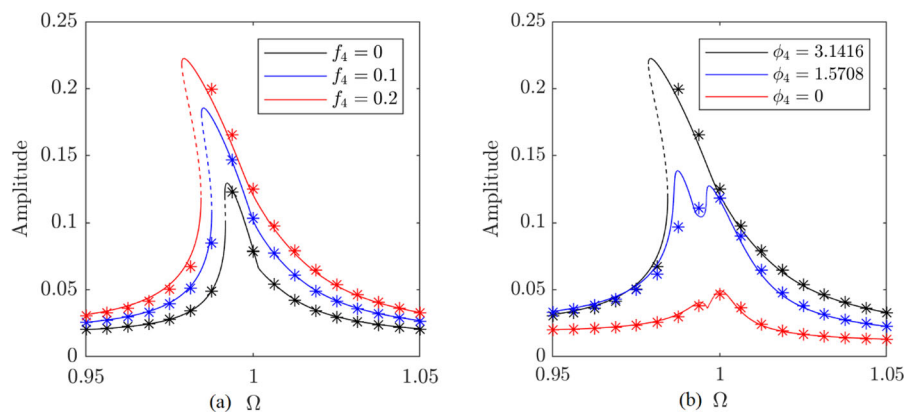
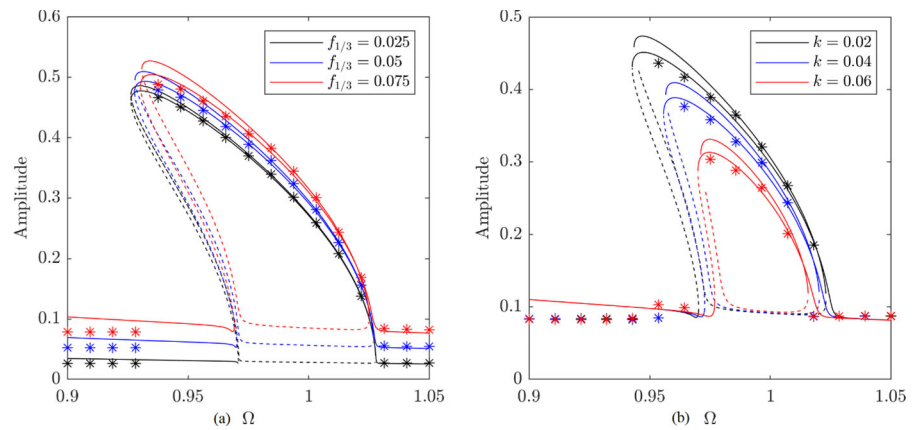


Fig. 16 Effect of **a** amplitude and **b** phase of the 4:1 superharmonic excitation on the frequency response of the uncontrolled system. Simulation results are marked by *. $\zeta_1 = 0.01, \zeta_2 = 1, \gamma_1 = 2.9053, \gamma_3 = 0.8174, \lambda_2 = 1.1575, f_1 = 0.001, f_3 = 0.1, f_4 = 0.2$

4.5 Simultaneous primary, principal parametric and self-excited resonance ($f_i = 0, i \neq \{1, 2\}, \zeta_1 < 0$)

The frequency response of the uncontrolled self-excited system subjected to both direct and parametric excitation is shown in Fig. 18. One observes a loop in the resonance plot. Such a system exhibits quasiperiodic response at frequencies away from the natural frequency due to secondary Hopf bifurcation (Neimer–Sacker bifurcation). It is evident that increasing the control gain progressively eliminates Hopf

bifurcation and hence the quasiperiodic oscillation as well as the loop in the resonance plot. The amplitude of oscillation can be reduced by a substantial margin by increasing the control gain. Figure 19 shows the time history of the system response with and without control.

4.6 Controlling chaos ($f_i = 0, i \neq \{1, 1/3, 3, 4\}, \zeta_1 < 0$)

It is well known that a chaotic response is possible in the system considered here. In the present section, an

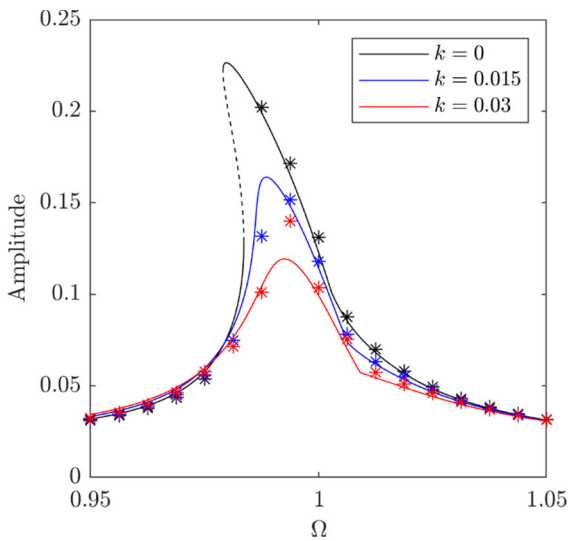


Fig. 17 Effect of control gain on the frequency response of the system. $\zeta_1 = 0.01$, $\zeta_2 = 1$, $\gamma_1 = 2.9053$, $\gamma_3 = 0.8174$, $\lambda_2 = 1.1575$, $f_1 = 0.001$, $f_3 = 0.1$, $f_4 = 0.2$, $k_a = 10$, $\zeta_f = 1$, $\Omega_f = 1$, $n = 1$

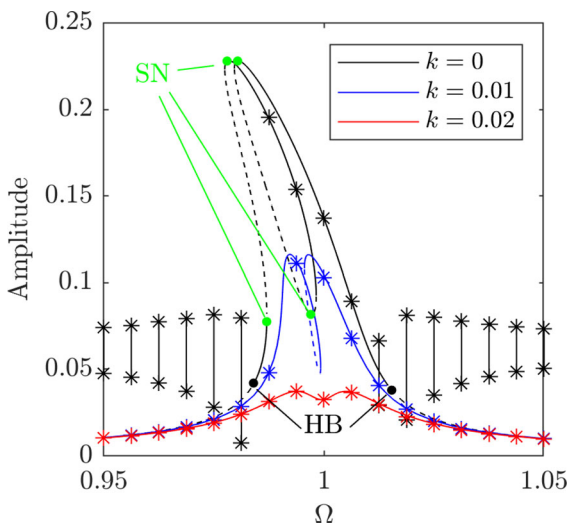


Fig. 18 Effect of gain on the Analytical (solid line) and Simulated (*) frequency response plots of the system subjected to both direct and parametric excitation. SN: saddle node bifurcation, HB: Hopf bifurcation, $\zeta_1 = -0.001$, $\zeta_2 = 1$, $\gamma_1 = 2.9053$, $\gamma_3 = 0.8174$, $\lambda_2 = 1.1575$, $f_2 = 0.02$, $k_a = 1$, $\zeta_f = 1$, $\Omega_f = 1$, $n = 10$

example is presented to demonstrate that the proposed controller can eliminate chaotic responses. To this end, a self-excited system with low nonlinear damping subjected to simultaneous 1/3 subharmonic, 3/1 superharmonic, primary, and 1/4 parametric subharmonic resonance is considered. Figure 20 depicts the frequency response of the uncontrolled system and the bifurcation points on it. It is evident from the bifurcation diagram shown in Fig. 21a that the uncontrolled system exhibits chaotic response at low and high frequencies around the resonance. It is further corroborated by the time history, phase portrait, FFT, and Poincare map of the system, for $\Omega = 0.85, 0.925, 1$ shown in Fig. 21b–d.

Figure 22 shows the response of the system with the proposed controller ($k = 0.05$). It can be observed that the proposed controller can suppress the chaotic behaviour of the system and establish the periodicity in the system response, which can also be verified from Fig. 23 depicting the variation of the maximum Lyapunov exponent (calculated using the *LET* toolbox [31]) with the control gain. Apparently, there exists a threshold value of the gain, k above which the maximum Lyapunov exponent is zero signifying the periodic system response.

4.7 Adaptive control

In the previous sections, the ratio of filter frequency to the system’s natural frequency is considered to be unity, i.e. filter frequency is set to the natural frequency of the system around which the system tends to oscillate. In case of an unknown natural frequency, Ω_f cannot be set to unity, and the filter is mistuned. To remove the dependence of filter frequency on the system parameter, one can tune it to the frequency of oscillation. This can be done manually. In order to tune the filter adaptively, the following adaptation law is used (The working principle of this equation is explained in “Appendix B”).

$$\frac{d\Omega_f}{dt} = k_b \text{sgn}(z)(\text{sgn}(\ddot{x}) - \text{sgn}(\dot{z})) \tag{20}$$

Fig. 19 Time history of the system response. The controller is switched on at $t = 1000$. $\zeta_1 = -0.001$, $\zeta_2 = 1$, $\gamma_1 = 2.9053$, $\gamma_3 = 0.8174$, $\lambda_2 = 1.1575$, $f_2 = 0.02$, $k_a = 1$, $\zeta_f = 1$, $\Omega_f = 1$, $n = 10$, $\Omega = 0.9812$

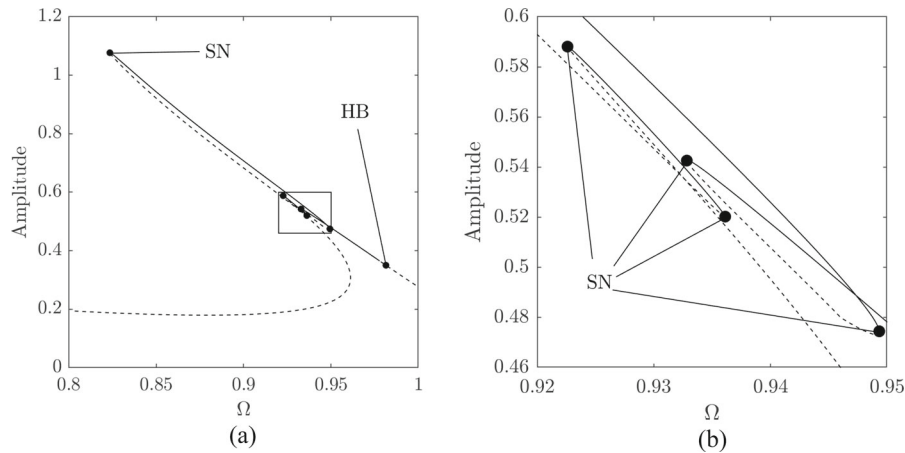
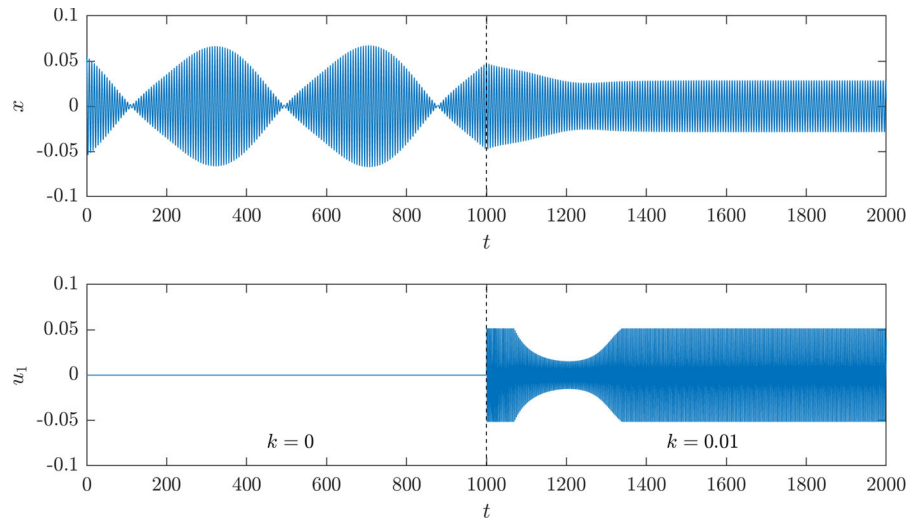


Fig. 20 **a** Frequency response of the uncontrolled self-excited system subjected to 1:3 direct subharmonic, 3:1 direct superharmonic, primary and 1:4 parametric subharmonic excitations and **b** zoomed-in view of the plot showing the boxed are in the plot **(a)**. SN: saddle node bifurcation. HB: Hopf

bifurcation. $\zeta_1 = -0.01$, $\zeta_2 = 0.2$, $\gamma_1 = 2.9053$, $\gamma_3 = 0.8174$, $\lambda_2 = 1.1575$, $f_1 = 0.01$, $f_2 = 0$, $f_3 = 0.05$, $f_4 = 0.1$, $f_{1/3} = 0.1$, $\phi_1 = 0$, $\phi_3 = 0$, $\phi_4 = 0$, $\phi_{1/3} = 0$

Figure 24 shows the time history of the system response as well as the output of the adaptation Eq. (20) and the control signal. It can be observed that a mistuned filter might amplify the existing vibrations. The proposed adaptive control successfully tunes the filter frequency and hence, achieves vibration reduction.

5 Experimental results

An axially excited stainless steel cantilever beam (30 cm × 2.5 cm × 0.5 cm) with a tip mass (~ 80 g, including the mass of accelerometers) is used as a test setup for the experiment, as shown in Fig. 25. The components used for the experiment and

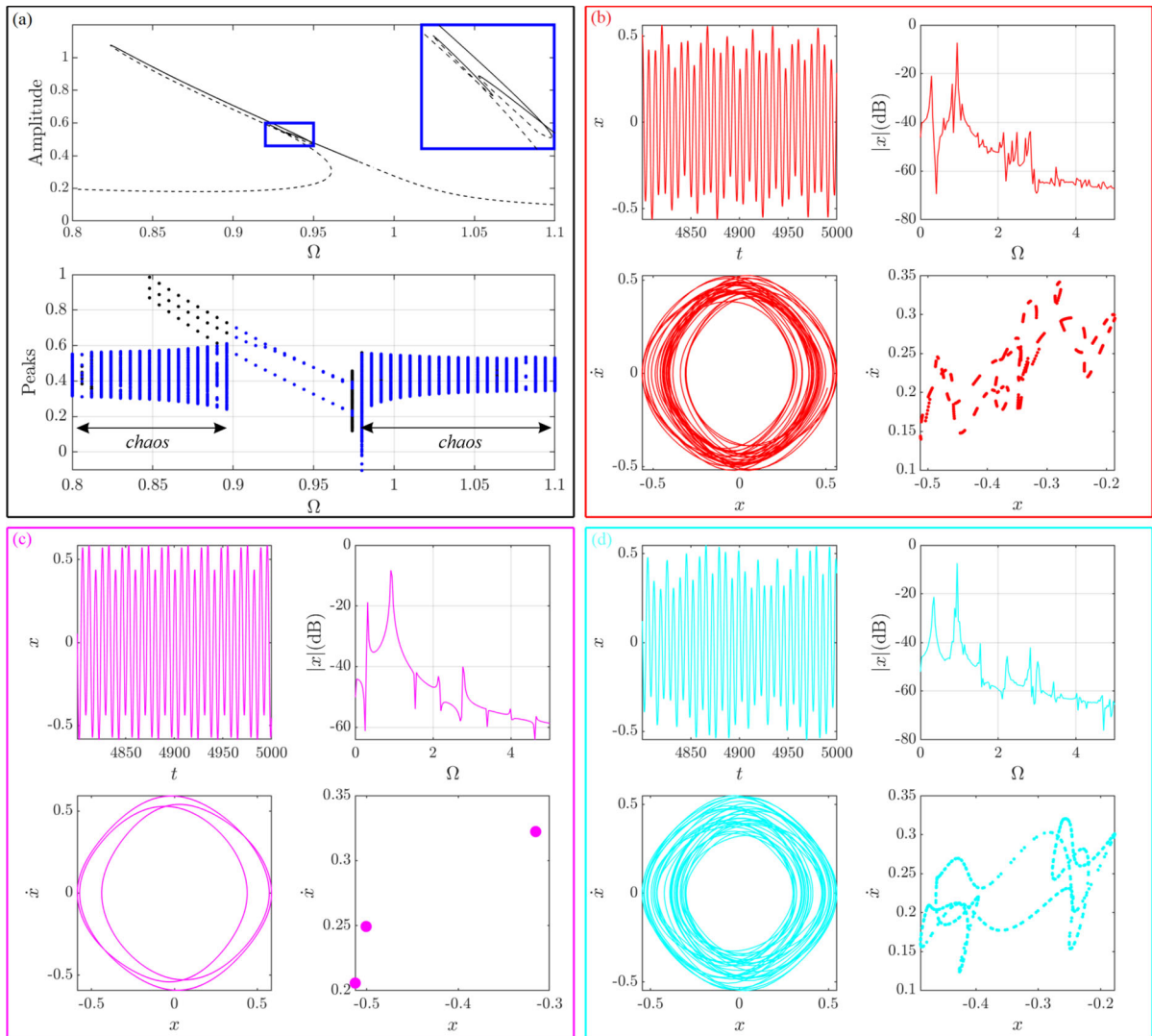


Fig. 21 a Frequency response and Bifurcation diagram (black for the backward sweep and blue for the forward sweep), time history, FFT, Phase portrait and Poincare map at $\Omega = 0.825$ (red, b), $\Omega = 0.925$ (magenta, c) and $\Omega = 1$ (cyan, d) of an

uncontrolled system. $\zeta_1 = -0.01$, $\zeta_2 = 0.2$, $\gamma_1 = 2.9053$, $\gamma_3 = 0.8174$, $\lambda_2 = 1.1575$, $f_1 = 0.01$, $f_2 = 0$, $f_3 = 0.05$, $f_4 = 0.1$, $f_{1/3} = 0.1$, $\phi_1 = 0$, $\phi_3 = 0$, $\phi_4 = 0$, $\phi_{1/3} = 0$, $k_a = 1$, $\zeta_f = 1$, $\Omega_f = 1$, $n = 1$, $k = 0$

their specifications are given in Table 1. The actuator shown in Fig. 25 is used for excitation and control, i.e., the signal fed to the actuator consists of excitation and control signals.

The control signal and the output of Eq. (3e), i.e. k_{11} is shown in Fig. 26. The shape of the control signal

matches with the simulated control signal as shown in Fig. 2. Figure 27 shows the output of Eq. (3d), which is supposed to be a unit amplitude signal with zero phase shift. From Figs. 26 and 27, it can be concluded that the equations designed in this article for getting a unit amplitude signal with zero phase shift and for

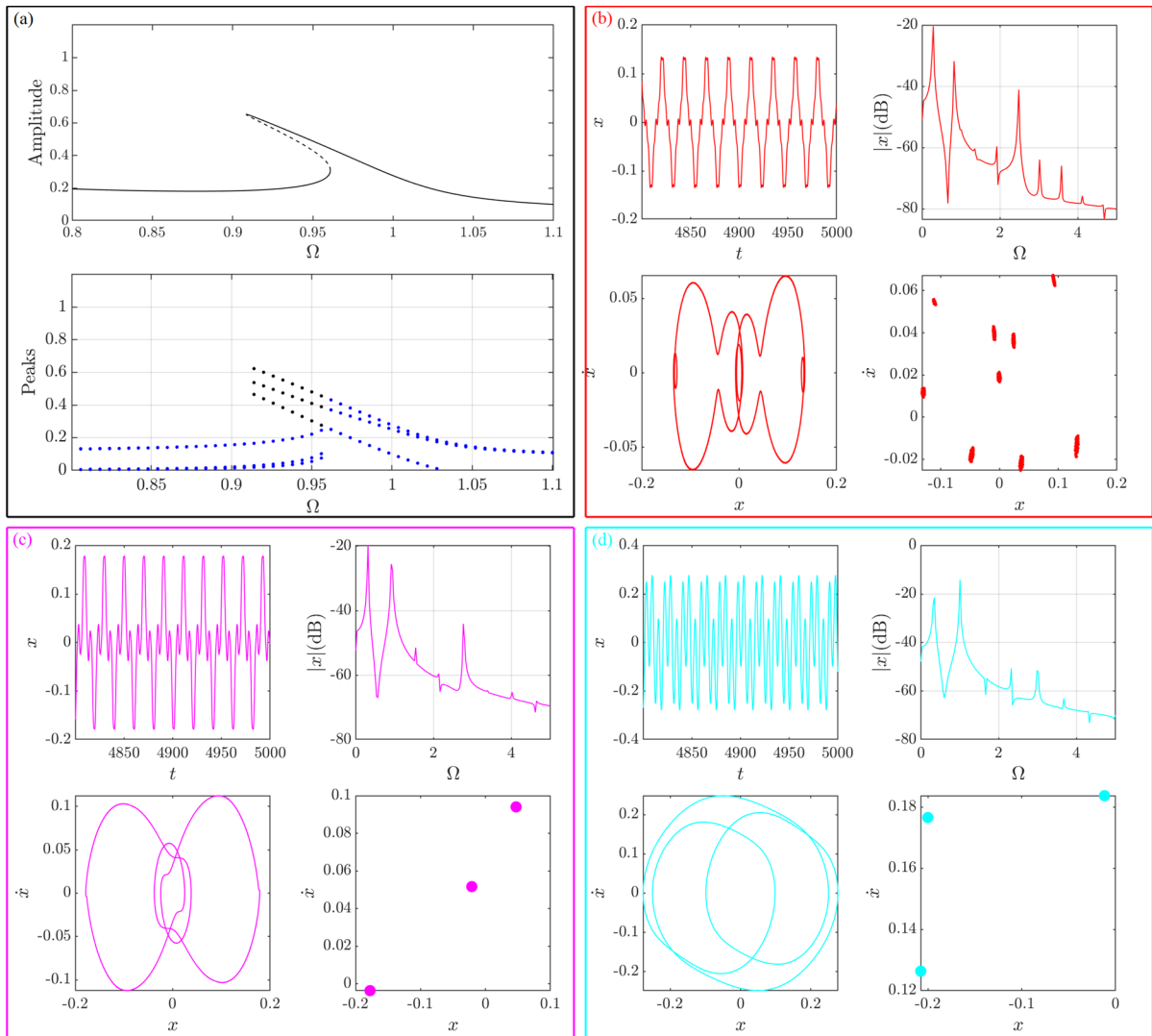


Fig. 22 **a** Frequency response and Bifurcation diagram(black), time history, FFT, Phase portrait and Poincare map at $\Omega = 0.825$ (red, **b**), $\Omega = 0.925$ (magenta, **c**) and $\Omega = 1$ (cyan, **d**) of the system with controller. $\zeta_1 = -0.01$, $\zeta_2 = 0.2$, $\gamma_1 = 2.9053$,

$\gamma_3 = 0.8174$, $\lambda_2 = 1.1575$, $f_1 = 0.01$, $f_2 = 0$, $f_3 = 0.05$, $f_4 = 0.1$, $f_{1/3} = 0.1$, $\phi_1 = 0$, $\phi_3 = 0$, $\phi_4 = 0$, $\phi_{1/3} = 0$, $k_a = 1$, $\zeta_f = 1$, $\Omega_f = 1$, $n = 1$, $k = 0.05$

obtaining an approximated *cotangent* wave from a *cosine* wave fulfill the objective.

The output of Eq. (3e) and (3c) are shown in Fig. 28 for both uncontrolled and controlled systems. Whereas Fig. 29 shows the recorded system response

(acc) during the experiment. The controller is switched on at $t \approx 750$ s. It can be observed that the proposed control fully suppresses the parametric resonance.

Figure 30 shows the frequency response of the system with and without control. The experimental

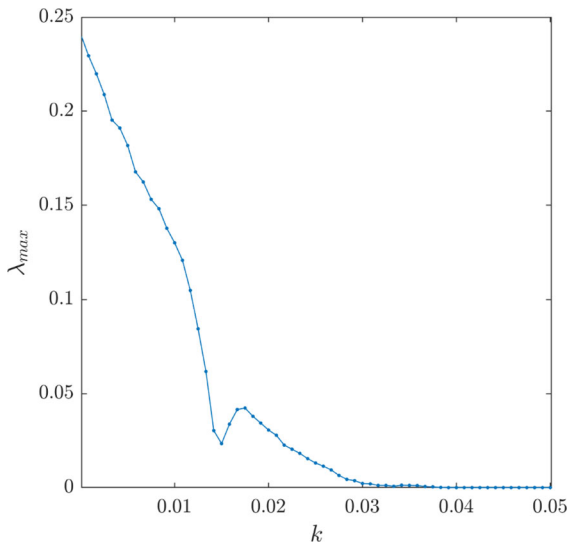
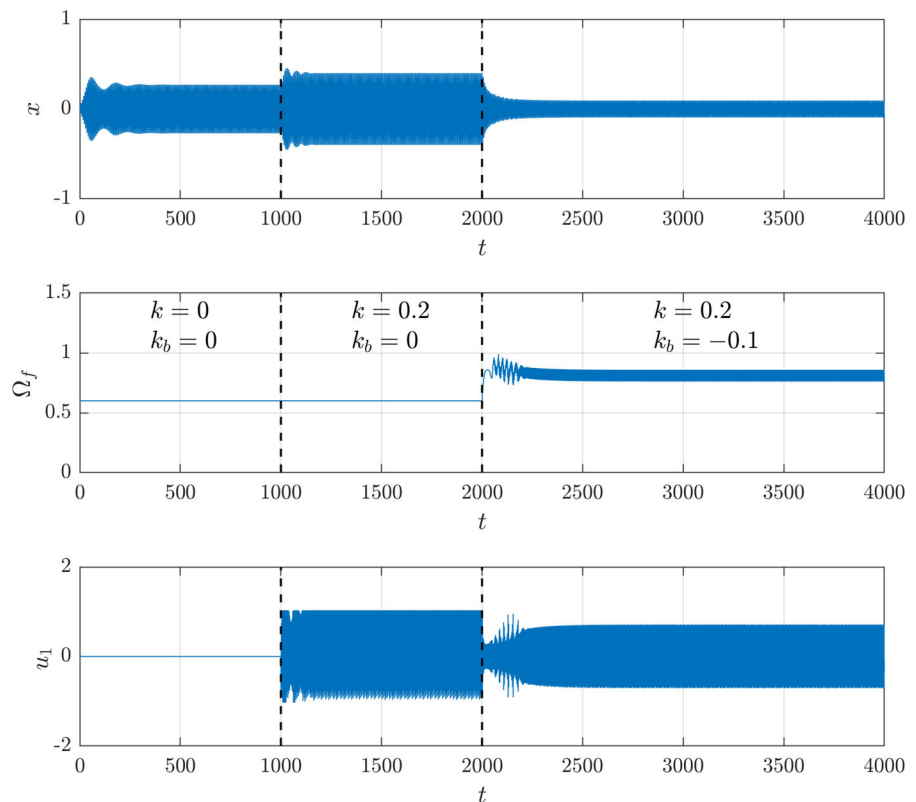


Fig. 23 Variation of maximum Lyapunov exponent with increasing gain. $\zeta_1 = -0.01$, $\zeta_2 = 0.2$, $\gamma_1 = 2.9053$, $\gamma_3 = 0.8174$, $\lambda_2 = 1.1575$, $f_1 = 0.01$, $f_2 = 0$, $f_3 = 0.05$, $f_4 = 0.1$, $f_{1/3} = 0.1$, $\phi_1 = 0$, $\phi_3 = 0$, $\phi_4 = 0$, $\phi_{1/3} = 0$, $k_a = 1$, $\zeta_f = 1$, $\Omega_f = 1$, $n = 1$, $\Omega = 0.9$

Fig. 24 Time history of the system response x , filter frequency Ω_f , and control signal u_1 . The control is switched on at $t = 1000$ with a mistuned filter ($\Omega_f = 0.6$). The adaptive control is activated at $t = 2000$, $\zeta_1 = -0.01$, $\zeta_2 = 1$, $\gamma_1 = 2.9053$, $\gamma_3 = 0.8174$, $\lambda_2 = 1.1575$, $f_1 = 0.01$, $f_2 = 0.1$, $f_3 = 0.05$, $f_4 = 0.05$, $f_{1/3} = 0$, $\phi_1 = 0$, $\phi_3 = 0$, $\phi_4 = 0$, $\phi_{1/3} = 0$, $k_a = 1$, $\zeta_f = 1$, $n = 10$



results are in close agreement with the analytical and simulation results shown in Fig. 4.

6 Conclusions

In this paper, a novel Resonant Parametric Feedback Controller (RPFC) is proposed to improve the system’s damping via parametric variations and suppress various nonlinear resonances and chaos in a cantilever beam. The cantilever beam is subjected to 1:1 direct excitation, 1:3 subharmonic direct excitation, 3:1 super harmonic direct excitation, 1:2 parametric excitation, 1:4 subharmonic parametric excitation, and self-excitation. The controller consists of a linear second-order filter with acceleration feedback and a novel control law which is a nonlinear function of the state variables of the filter. The effectiveness of the proposed controller is studied for the following cases.

1. Principal parametric resonance
2. Direct resonances—primary, 1/3 subharmonic and 3/1 superharmonic.
3. Self-excited systems

Fig. 25 Experimental setup

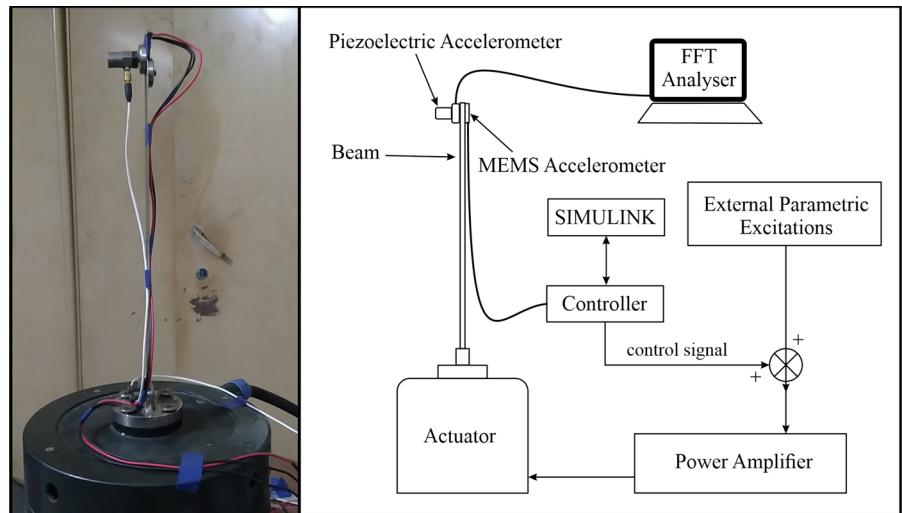
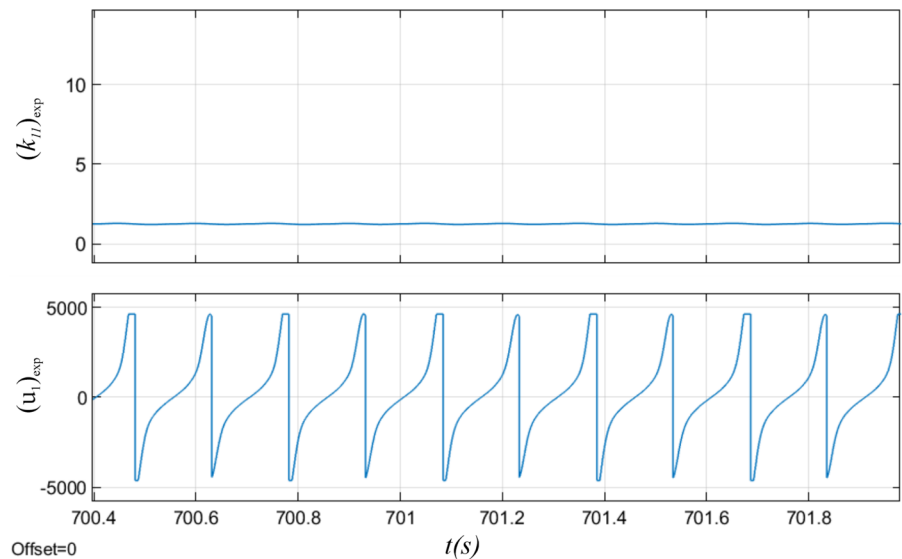


Table 1 List of equipment and their uses

Equipment	Model	Use
Accelerometers	ADXL335 (MEMS)	Feedback
	PCB Piezotronics(Piezoelectric)	Real time monitoring
Microcontroller	TI C2000-F28379D	Signal processing and data logging
Analyzer	B&K pulse PC card front end	Real-time FFT
Power amplifier	B&K type 2719	Power amplification of the control signal

Fig. 26 The output of Eq. (3e) and control signal at a steady state. (Experimental) $n = 10$



4. Various combinations of simultaneous direct and parametric and self-excited resonances.

From the analytical solutions and the numerical simulations, it is concluded that the proposed

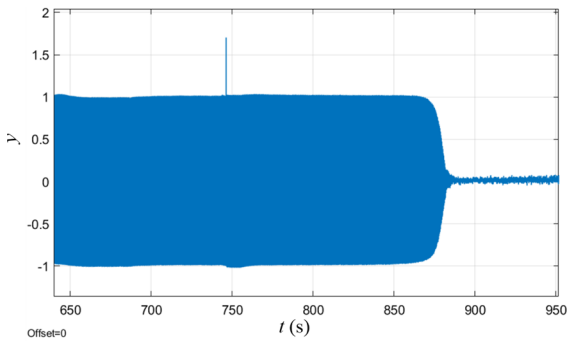


Fig. 27 Output of Eq. (3d). (Experimental). The controller is activated at $t \approx 750$ s. $n = 10$

Fig. 28 Variation of k_{11} and control signal with time (Experimental). The controller is activated at $t \approx 750$ s. $n = 10$

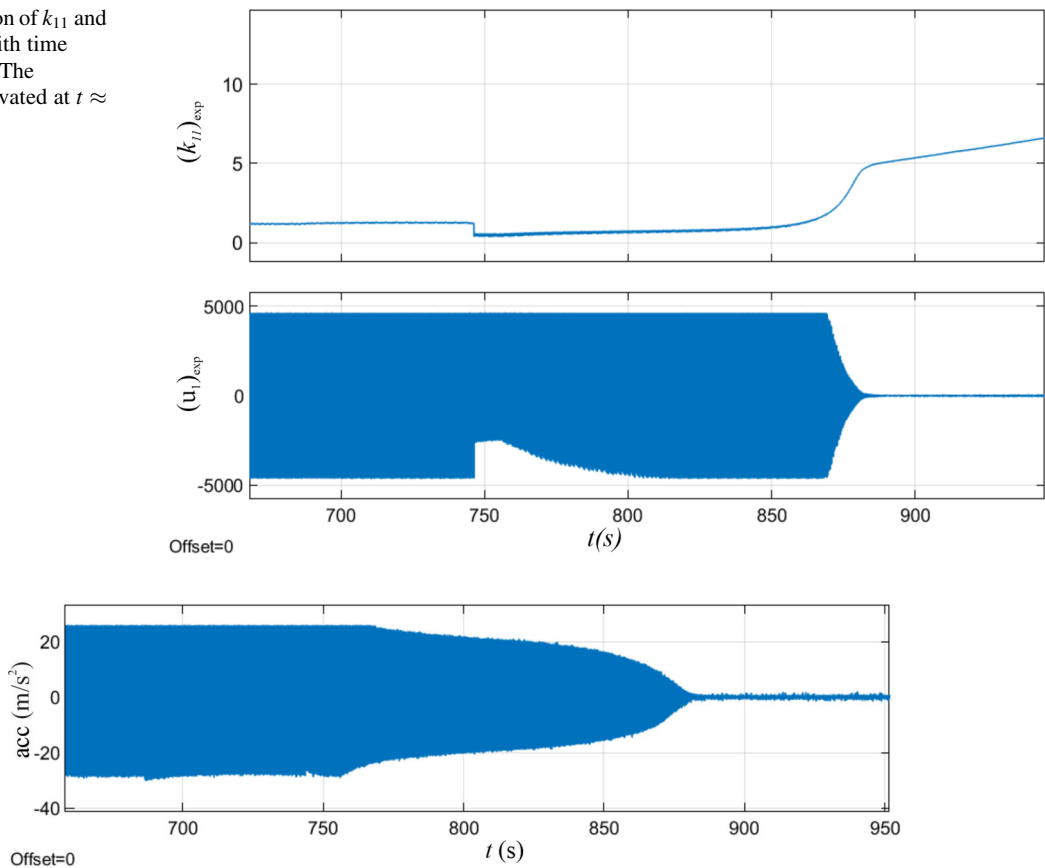


Fig. 29 System response (Experimental). The controller is activated at $t \approx 750$ s. $n = 10$

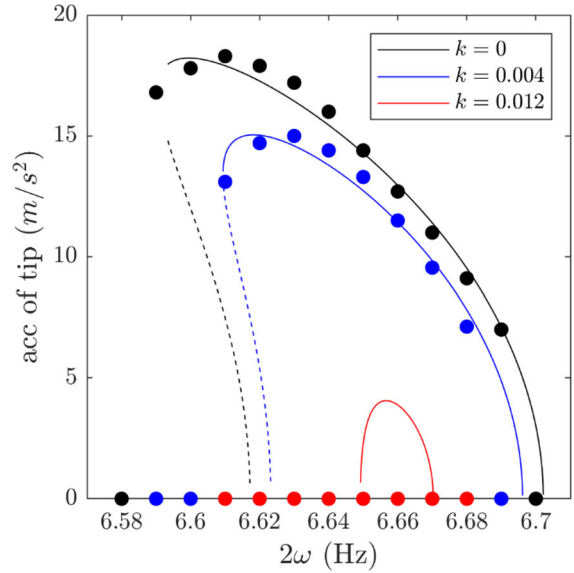


Fig. 30 Experimental frequency response of the system

controller suppresses the nonlinear resonances and eliminates the quasiperiodic and chaotic behaviour from the system. The results for suppression of the principal parametric resonance are verified by experiments.

Further, a novel adaptation law is proposed to deal with the uncertainties in the system's natural frequency. The proposed adaptation law tunes the filter frequency such that the phase difference between the dominating harmonic component of the input signal and the filter output is $\pi/2$. From simulation results, it can be observed that a mistuned controller can amplify the system response. Introducing the adaptation law achieves a reduction in the amplitude of the system response.

Author contribution All authors contributed to the study conception and design. Material preparation, data collection and analysis were performed by [full name], [full name] and [full name]. The first draft of the manuscript was written by [full name] and all authors commented on previous versions of the manuscript. All authors read and approved the final manuscript.

Funding The authors declare that no funds, grants, or other support were received during the preparation of this manuscript.

Data availability No data are used for the present study.

Declarations

Competing interests The authors have no relevant financial or non-financial interests to disclose.

Appendix A

Derivation of the governing equation of a cantilever beam vibrating due to the axial and transverse motion of the base.

List of variables used:

w	Transverse deflection of the beam
u	Axial deflection of the beam
s	Coordinate along the length of the beam
ρ	Density of the beam
A	Cross section area of the beam
L	Length of the cantilever beam
m	Tip mass

x_e	Axial displacement of base/support
y_e	Transverse displacement of base/support
v_s	Normalized mode shape of the beam
v	Time dependent scaling factor
ω_n	First mode of the beam

Strain energy

$$U = \frac{1}{2} \int_0^l \int_A E z^2 \kappa^2 dA ds, \quad (\text{A.1})$$

where z is the distance from the neutral axis, and κ is the curvature. Assuming that the beam is inextensible

$$\begin{aligned} \kappa &= \frac{\partial}{\partial s} \alpha(s, t) \\ &= w^{(2,0)}(s, t) + \frac{1}{2} w^{(2,0)}(s, t) w^{(1,0)}(s, t)^2 + \dots \end{aligned} \quad (\text{A.2})$$

where $w(s, t)$ is the transverse displacement at a distance s from the fixed end and $w^{(i,j)}(s, t) = \frac{\partial^i}{\partial s^i} \left(\frac{\partial^j w}{\partial t^j} \right)$

Substituting Eq. (A2) in Eq. (A1) and neglecting the higher order terms,

$$U = \frac{1}{2} \int_0^l \int_A E z^2 \left([w^{(2,0)}(s, t)]^2 + [w^{(2,0)}(s, t) w^{(1,0)}(s, t)]^2 \right) dA ds \quad (\text{A.3})$$

$$\begin{aligned} U &= \frac{1}{2} \int_0^l EI [w^{(2,0)}(s, t)]^2 ds \\ &+ \frac{1}{2} \int_0^l EI [w^{(1,0)}(s, t) w^{(2,0)}(s, t)]^2 ds \end{aligned} \quad (\text{A.4})$$

Applying the variational operator,

$$\begin{aligned} \delta U &= \int_0^L EI \left[w^{(2,0)}(s, t) \left(1 + (w^{(1,0)}(s, t))^2 \right) \right] \delta w^{(2,0)}(s, t) ds \\ &+ \int_0^l EI \left[w^{(1,0)}(s, t) (w^{(2,0)}(s, t))^2 \delta w^{(1,0)}(s, t) \right] ds \end{aligned} \quad (\text{A.5})$$

Integrating by parts one obtains

Inextensibility constraint

$$\delta U = EI \left(\begin{aligned} & \left(w^{(2,0)}(s,t) \left(1 + \left(w^{(1,0)}(s,t) \right)^2 \right) \delta w^{(1,0)}(s,t) \right)_0^L \\ & - \left(\left(w^{(3,0)}(s,t) \left(1 + \left(w^{(1,0)}(s,t) \right)^2 \right) + w^{(1,0)}(s,t) \left(w^{(2,0)}(s,t) \right)^2 \right) \delta w(s,t) \right)_0^L \\ & + \int_0^L \left(w^{(4,0)}(s,t) \left(1 + \left(w^{(1,0)}(s,t) \right)^2 \right) + \left(w^{(2,0)}(s,t) \right)^3 \right. \\ & \quad \left. + 4w^{(1,0)}(s,t)w^{(2,0)}(s,t)w^{(3,0)}(s,t) \right) \delta w(s,t) ds \end{aligned} \right) \tag{A.6}$$

$$\begin{aligned} (1 + u^{(1,0)}(s,t))^2 + w^{(1,0)}(s,t)^2 &= 1 \\ C &= \int_0^L \frac{\lambda}{2} \left(1 - \left(1 + u^{(1,0)}(s,t) \right)^2 - w^{(1,0)}(s,t)^2 \right) ds, \end{aligned} \tag{A.7}$$

where λ is a Lagrange multiplier. Applying variational operator to the Eq. (A7) and integrating by parts yields,

$$\begin{aligned} \delta C &= \left[-\lambda \left(\left(1 + u^{(1,0)}(s,t) \right) \delta u(s,t) + w^{(1,0)}(s,t) \delta w(s,t) \right) \right]_0^L \\ &+ \int_0^L \left(\left(\lambda \left(1 + u^{(1,0)}(s,t) \right) \right)' \delta u(s,t) \right. \\ &\left. + \left(\lambda w^{(2,0)}(s,t) + \lambda' w^{(1,0)}(s,t) \right) \delta w(s,t) \right) ds \end{aligned} \tag{A.8}$$

Kinetic energy

$$\begin{aligned} T &= \frac{1}{2} m \int_0^L \left([\dot{x}_e + \dot{u}]^2 + [\dot{y}_e + \dot{w}]^2 \right) \delta^*(s-L) ds \\ &+ \frac{1}{2} \rho A \int_0^L \left([\dot{x}_e + \dot{u}]^2 + [\dot{y}_e + \dot{w}]^2 \right) ds, \end{aligned} \tag{A.9}$$

where δ^* is the Dirac delta function. Applying a variational operator to Eq. (A9) and integrating by parts, one obtains Eq.(A12)

$$\begin{aligned} \int_{t_1}^{t_2} \delta T dt &= -m \int_{t_1}^{t_2} \int_0^L \left([\ddot{u} + \ddot{x}_e] \delta u + [\ddot{w} + \ddot{y}_e] \delta w \right) \delta^*(s-L) ds dt \\ &- \rho A \int_{t_1}^{t_2} \int_0^L \left([\ddot{u} + \ddot{x}_e] \delta u + [\ddot{w} + \ddot{y}_e] \delta w \right) ds dt \end{aligned} \tag{A.10}$$

Hamilton’s principle

$$\delta \int_{t_1}^{t_2} (T - (U + V) + C) dt = 0 \tag{A.11}$$

Substituting Eq. (A6), (A8), and (A10) in eq. (A11) one obtains Eq. (A12)

Boundary conditions

From Eq. (A12) following boundary conditions are obtained.

At $s = 0$

$$w^{(1,0)}(0,t) = 0 \tag{A.13}$$

$$u(0,t) = 0 \tag{A.14}$$

$$w(0,t) = 0 \tag{A.15}$$

At $s = L$

$$w^{(2,0)}(L,t) = 0 \tag{A.16}$$

$$\begin{aligned}
 \int_{t_1}^{t_2} (\delta T - \delta U + \delta C) dt &= -m \int_{t_1}^{t_2} ([\ddot{u} + \ddot{x}_e] \delta u + [\ddot{w} + \ddot{y}_e] \delta w)_{s=L} dt \\
 &- \rho A \int_{t_1}^{t_2} \int_0^L ([\ddot{u} + \ddot{x}_e] \delta u + [\ddot{w} + \ddot{y}_e] \delta w) ds dt \\
 &- \int_{t_1}^{t_2} EI \left(\begin{aligned} &\left(\left[w^{(2,0)}(s,t) \left(1 + \left(w^{(1,0)}(s,t) \right)^2 \right] \right) \delta w^{(1,0)}(s,t) \right)_0^L \\ &- \left(\left[w^{(3,0)}(s,t) \left(1 + \left(w^{(1,0)}(s,t) \right)^2 \right) + w^{(1,0)}(s,t) \left(w^{(2,0)}(s,t) \right)^2 \right] \delta w(s,t) \right)_0^L \\ &+ \int_0^L \left[\begin{aligned} &w^{(4,0)}(s,t) \left(1 + \left(w^{(1,0)}(s,t) \right)^2 \right) + \left(w^{(2,0)}(s,t) \right)^3 \\ &+ 4w^{(1,0)}(s,t)w^{(2,0)}(s,t)w^{(3,0)}(s,t) \end{aligned} \right] \delta w(s,t) ds \end{aligned} \right) dt \tag{A.12} \\
 &- \int_{t_1}^{t_2} \left[\lambda \left(\left(1 + u^{(1,0)}(s,t) \right) \delta u(s,t) + w^{(1,0)}(s,t) \delta w(s,t) \right) \right]_0^L dt \\
 &+ \int_{t_1}^{t_2} \int_0^L \left(\left(\lambda \left(1 + u^{(1,0)}(s,t) \right) \right)' \delta u(s,t) + \left(\lambda w^{(1,0)}(s,t) \right)' \delta w(s,t) \right) ds dt
 \end{aligned}$$

$$\lambda = - \frac{m(\ddot{u} + \ddot{x}_e)}{1 + u^{(1,0)}(s,t)} \tag{A.17}$$

$$c(t) = - \left[m(\ddot{u} + \ddot{x}_e) + \int_0^s \rho A (\ddot{u} + \ddot{x}_e) ds \right]_{s=L} \tag{A.22}$$

$$\begin{aligned}
 EI w^{(3,0)}(s,t) &= \frac{m}{1 + \left(w^{(1,0)}(s,t) \right)^2} \\
 &\left((\ddot{w} + \ddot{y}_e) - (\ddot{u} + \ddot{x}_e) \left(\frac{w^{(1,0)}(s,t)}{1 + u^{(1,0)}(s,t)} \right) \right) \tag{A.18}
 \end{aligned}$$

From Eq. (A21) and (A22) the Lagrange multiplier is obtained as

$$\lambda = \frac{-1}{1 + u'} \left(m(\ddot{u} + \ddot{x}_e)_{s=L} + \rho A \int_s^L (\ddot{u} + \ddot{x}_e) ds \right) \tag{A.23}$$

Equations of motion

From Eq. (A12) following equations of motion are obtained

$$\begin{aligned}
 -\rho A (\ddot{u} + \ddot{x}_e) + (\lambda(1 + u'))' &= 0 \tag{A.19} \\
 -\rho A (\ddot{w} + \ddot{y}_e) + (\lambda w')' \\
 -EI \left(\begin{aligned} &w^{(4,0)}(s,t) \left(1 + \left(w^{(1,0)}(s,t) \right)^2 \right) + \left(w^{(2,0)}(s,t) \right)^3 \\ &+ 4w^{(1,0)}(s,t)w^{(2,0)}(s,t)w^{(3,0)}(s,t) \end{aligned} \right) &= 0 \tag{A.20}
 \end{aligned}$$

From Eq. (A19)

$$\lambda(1 + u') = \int_0^s \rho A (\ddot{u} + \ddot{x}_e) ds + c(t) \tag{A.21}$$

From Eqs. (A17) and (A21)

Substituting Eq. (A23) and $u = \int_0^s (\sqrt{1 - w^2} - 1) ds \approx \int_0^s (-w^2/2) ds$ in Eq. (A20), following equation is obtained

$$\begin{aligned}
 \rho A (\ddot{w} + \ddot{y}_e) &+ \left(\frac{(1 - 2w^2)w'}{(1 - w^2)^{3/2}} \left(m \left(\frac{\partial^2}{\partial t^2} \left(\int_0^s (-w^2/2) ds \right) + \ddot{x}_e \right)_{s=L} \right) \right) \\
 &+ \rho A \int_s^L \left(\frac{\partial^2}{\partial t^2} \left(\int_0^s (-w^2/2) ds \right) + \ddot{x}_e \right) ds \\
 -\rho A \frac{w'}{\sqrt{1 - w^2}} \left(\frac{\partial^2}{\partial t^2} \left(\int_0^s (-w^2/2) ds \right) + \ddot{x}_e \right) \\
 + EI \left(\begin{aligned} &w^{(4,0)}(s,t) \left(1 + \left(w^{(1,0)}(s,t) \right)^2 \right) + \left(w^{(2,0)}(s,t) \right)^3 \\ &+ 4w^{(1,0)}(s,t)w^{(2,0)}(s,t)w^{(3,0)}(s,t) \end{aligned} \right) &= 0 \tag{A.24}
 \end{aligned}$$

Using Binomial expansion Eq. (A24) can be simplified to the following equation

$$\begin{aligned} &\rho A(\ddot{w} + \ddot{y}_e) + \left((1 - 2w^2)w'' \left(1 + \frac{3}{2}w^2 \right) \left(\begin{aligned} &m \left(\frac{\partial^2}{\partial t^2} \left(\int_0^s (-w^2/2) ds \right) + \ddot{x}_e \right)_{s=L} \right) \\ &+ \rho A \int_s^L \left(\frac{\partial^2}{\partial t^2} \left(\int_0^s (-w^2/2) ds \right) + \ddot{x}_e \right) ds \end{aligned} \right) \right) \\ &- \rho A \frac{w'}{\sqrt{1-w^2}} \left(1 + \frac{1}{2}w^2 \right) \left(\frac{\partial^2}{\partial t^2} \left(\int_0^s (-w^2/2) ds \right) + \ddot{x}_e \right) \\ &+ EI \left(\begin{aligned} &w^{(4,0)}(s,t) \left(1 + \left(w^{(1,0)}(s,t) \right)^2 \right) + \left(w^{(2,0)}(s,t) \right)^3 \\ &+ 4w^{(1,0)}(s,t)w^{(2,0)}(s,t)w^{(3,0)}(s,t) \end{aligned} \right) = 0 \end{aligned} \tag{A.25}$$

Neglecting the higher order terms,

$$\begin{aligned} &\rho A(\ddot{w} + \ddot{y}_e) + w'' \left(\begin{aligned} &m \left(\frac{\partial^2}{\partial t^2} \left(\int_0^L (-w^2/2) ds \right) + \ddot{x}_e \right) \\ &+ \rho A \int_s^L \left(\frac{\partial^2}{\partial t^2} \left(\int_0^s (-w^2/2) ds \right) + \ddot{x}_e \right) ds \end{aligned} \right) \\ &- \rho A w' \left(\frac{\partial^2}{\partial t^2} \left(\int_0^s (-w^2/2) ds \right) + \ddot{x}_e \right) \\ &+ EI \left(\begin{aligned} &w^{(4,0)}(s,t) \left(1 + \left(w^{(1,0)}(s,t) \right)^2 \right) + \left(w^{(2,0)}(s,t) \right)^3 \\ &+ 4w^{(1,0)}(s,t)w^{(2,0)}(s,t)w^{(3,0)}(s,t) \end{aligned} \right) = 0 \end{aligned} \tag{A.26}$$

Separating the variables assuming that the beam vibrates around the first mode

$$w(s, t) = v_s(s)v(t) \tag{A.27}$$

where v_s is the mode shape function at first mode. Substituting the above equation in Eq. (A.26)

$$\begin{aligned} &\rho A v_s \ddot{v} + v(v\ddot{v} + \dot{v}^2) \left(-m v_{s2} \left(\int_0^L v_{s1}^2 ds \right) \right. \\ &+ \rho A v_{s1} \left(\int_0^s v_{s1}^2 ds \right) - \rho A v_{s2} \int_s^L \int_0^s v_{s1}^2 ds ds \\ &+ (m v_{s2} + \rho A (v_{s2}(L-s) - v_{s1})) v \ddot{x}_e + \rho A \ddot{y}_e \\ &+ EI v v_{s4} + EI v^3 (v_{s4} v_{s1}^2 + v_{s2}^3 + 4v_{s1} v_{s2} v_{s3}) = R \end{aligned} \tag{A.28}$$

where R is the residual.

After Galerkin projection, the above equation can be expressed as

$$\hat{\gamma}_0 \ddot{v} + \hat{\gamma}_1 (v^2 + v\dot{v})v + \hat{\gamma}_2 v + \hat{\gamma}_3 v^3 + \hat{\lambda}_2 v \ddot{x}_e + \hat{\lambda}_1 \ddot{y}_e = 0 \tag{A.29}$$

where

$$\begin{aligned} \hat{\gamma}_0 &= \rho A \int_0^L v_s^2 ds \\ \hat{\gamma}_1 &= \int_0^L v_s \left(\rho A v_{s1} \int_0^s v_{s1}^2 ds - v_{s2} \left(m \int_0^L v_{s1}^2 ds \right. \right. \\ &\quad \left. \left. + \rho A \int_s^L \int_0^s v_{s1}^2 ds ds \right) \right) ds \\ \hat{\gamma}_2 &= EI \int_0^L v_s v_{s4} ds \\ \hat{\gamma}_3 &= EI \int_0^L v_s (v_{s4} v_{s1}^2 + v_{s2}^3 + 4v_{s1} v_{s2} v_{s3}) ds \\ \hat{\lambda}_1 &= \rho A \int_0^L v_s ds \\ \hat{\lambda}_2 &= \int_0^L m v_{s2} v_s ds + \int_0^L \rho A v_s (v_{s2}(L-s) - v_{s1}) ds \end{aligned}$$

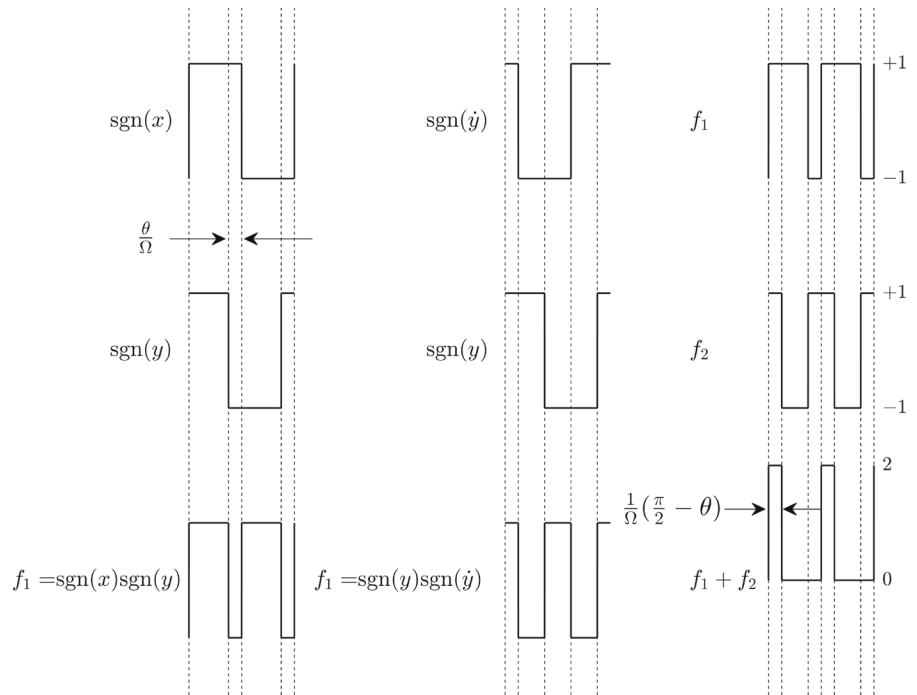
The above equation when converted to the non-dimensional form, gives the following equation

$$\ddot{x} + \gamma_1 (x^2 + x\dot{x})x + x + \gamma_3 x^3 = \lambda_2 F_2 x + F_1 \tag{A.30}$$

where $v = Lx$, $\tau = \omega_n t$ and ω_n is the first mode of the system and is given by,

$$\begin{aligned} \omega_n^2 &= \frac{\hat{\gamma}_2}{\hat{\gamma}_0} = \frac{EI \int_0^L v_s v_{s4} ds}{\rho A \int_0^L v_s^2 ds} \\ &= \frac{EI}{\rho A L^4} \frac{\int_0^1 v_p v_{p4} dp}{\int_0^1 v_p^2 dp} \end{aligned}$$

Fig. 31 Graphical representation of the adaptation equation



where v_p is a normalized mode shape and v_{pi} denotes the i^{th} derivative of v_p .

The non-dimensional parameters from Eq. (A28) can be obtained from the following expressions

$$\gamma_1 = \frac{\hat{\gamma}_1}{\hat{\gamma}_0} L^2 = \frac{\gamma_{11} - m_r \gamma_{12}}{\gamma_{13}}$$

where m_r is the ratio of mass at the tip and the total mass of beam.

$$\gamma_{11} = \int_0^1 \left(v_p v_{p1} \int_0^p v_{p1}^2 dp \right) dp - \int_0^1 \left(v_p v_{p2} \int_p^1 \left(\int_0^p v_{p1}^2 dp \right) dp \right) dp$$

$$\gamma_{12} = \int_0^1 \left(v_p v_{p2} \int_0^1 v_{p1}^2 dp \right) dp$$

$$\gamma_{13} = \int_0^1 v_p^2 dp$$

$$\gamma_3 = \frac{\hat{\gamma}_3}{\hat{\gamma}_2} L^2 = \frac{\int_0^1 v_p (v_{p4} v_{p1}^2 + v_{p2}^3 + 4v_{p1} v_{p2} v_{p3}) dp}{\int_0^1 v_p v_{p4} dp}$$

$$\lambda_2 = -L \frac{\hat{\lambda}_2}{\hat{\gamma}_0} = \frac{\lambda_{21} + \lambda_{22} m_r}{\lambda_{23}}$$

$$\lambda_{21} = - \int_0^1 v_p (v_{p2} (1 - p) - v_{p1}) dp$$

$$\lambda_{22} = - \int_0^1 v_{p2} v_p dp$$

$$\lambda_{23} = \int_0^1 v_p^2 dp$$

Appendix B

The objective of introducing the adaptation equation is to maintain the phase difference between the displacement signal and the control signal at $\frac{\pi}{2}$ which results in improved damping irrespective of the excitation frequency. The phase difference can be adjusted by tuning the filter frequency. The product of two harmonic signals with the same frequency (ω , say) gives a biased signal with 2ω frequency. The bias is directly proportional to the cosine of the phase difference between the input signals. Using this property, a first-order differential equation can be constructed as follows

$$\frac{d\Omega_f}{dt} = k_b xy \tag{B.1}$$

The rate of convergence for this equation depends on the amplitudes of the system variable and the control force. This leads to a slow response of the adaptation equation for low amplitude vibration suppression. To make the adaptation law independent of the amplitudes, a signum function is used, as shown in Eq. (B.2)

$$\frac{d\Omega_f}{dt} = k_b \text{sgn}(x)\text{sgn}(y) \tag{B.2}$$

Equation (B.2) is shown graphically in Fig. 31. One can observe that at a steady state, the right-hand side of the adaptation equation gives a square wave which results in the chattering of filtering frequency. To remove this chattering, another square wave is added to the right-hand side of the adaptation equation but with the phase difference of π radians. This secondary square wave is generated from the already available state variables of the filter. The modified adaptation law is,

$$\frac{d\Omega_f}{dt} = k_b (\text{sgn}(x)\text{sgn}(y) + \text{sgn}(y)\text{sgn}(\dot{y})) \tag{B.3}$$

Addition of secondary square wave results in either positive or negative pulses. Where pulse width is directly proportional to $(\frac{\pi}{2} - \theta)$ as shown in Fig. 31. This completely removes the chattering in theory and suppresses the chattering in practice.

For the signal dominated by a single frequency, $\text{sgn}(x)$ can be replaced by $-\text{sgn}(\ddot{x})$. Therefore, the same adaptation equation can be used for both displacement and acceleration signals.

$$\frac{d\Omega_f}{dt} = -k_b \text{sgn}(y)(\text{sgn}(\ddot{x}) - \text{sgn}(\dot{y})) \tag{B.4}$$

Here, $y = z$.

$$\frac{d\Omega_f}{dt} = k_b \text{sgn}(z)(\text{sgn}(\ddot{x}) - \text{sgn}(\dot{z})) \tag{B.5}$$

Appendix C

Procedure to calculate the coefficients c_i in Eqs. (2a) and (3e).

The approximated function is given by

$$u = \sum_{i=1}^n c_i (\cos(\Omega t + \alpha))^{2i-1} \text{sgn}(\sin(\Omega t + \alpha)) \tag{C.1}$$

The desired function is

$$u_0 = \cot(\Omega t + \alpha) \tag{C.2}$$

Since the polynomial approximation is independent of Ω , let $\Omega = 1$. Further shifting the time in the above signals, one obtains

$$u = \sum_{i=1}^n c_i (\cos t)^{2i-1} \text{sgn}(\sin t) \tag{C.3}$$

$$u_0 = \cot t \tag{C.4}$$

Since $\cot t$ is a periodic function with a period π , the error function is defined as

$$e_j = \sum_{i=1}^n c_i (\cos t_j)^{2i-1} - \cot t_j \quad t_j \in (0, \pi) \tag{C.5}$$

The above equation contains n variables. In order to apply the least square optimization method, n linearly spaced points are selected in the range $t \in (0, \pi)$. This results in n error functions. The above optimization problem is then solved using the built-in MATLAB function *lsqnonlin*.

Appendix D

Consider a harmonic signal $z = a_{2,1} \sin(\Omega t)$. Squaring on both sides, one obtains,

$$z^2 = \frac{(a_{2,1})^2}{2} (1 - \cos(2\Omega t)) \tag{D.1}$$

Here, the objective is to find the controlling equation for a parameter (say $k_{11} > 0$) such that at steady state $k_{11}a_{2,1} = 1$. First, consider the lowest order of the differential equation. It is clear that the rate of change of k_{11} should be proportional to $[1 - (k_{11}a_{2,1})^2]$. So, the differential equation should look like this,

$$\dot{k}_{11} = k_{a1} [1 - (k_{11}a_{2,1})^2] \tag{D.2}$$

The problem in employing Eq. (D.2) is that the amplitude of the signal is unknown. But from Eq. (D.1) it is clear that the term z^2 consists of a bias and a periodic signal where bias is proportional to the

square of the amplitude of the signal. One can replace the term $(a_{2,1})^2$ with $2z^2$. There is a periodic component in z^2 , but the overall change in k_{11} due to this component over a time period $T = \frac{\pi}{\Omega}$ is zero. Therefore the governing equation for the parameter k_{11} is

$$\dot{k}_{11} = k_{a1} \left(1 - 2(k_{11}z)^2 \right) \quad (\text{D.3})$$

Or

$$\dot{k}_{11} = k_a \left(\frac{1}{2} - (k_{11}z)^2 \right) \quad (\text{D.4})$$

References

- Mathieu, É.: Mémoire sur le mouvement vibratoire d'une membrane de forme elliptique. *Journal de mathématiques pures et appliquées* **13**, 137–203 (1868)
- Blevins, R.D.: Models for vortex-induced vibration of cylinders based on measured forces. *J. Fluids Eng.* **131**, 10 (2009)
- Balas, M.J.: Direct velocity feedback control of large space structures. *J. Guid. Control* **2**(3), 252–253 (1979)
- Oueini, S.S., Nayfeh, H.A.: Single-mode control of a cantilever beam under principal parametric excitation. *J. Sound Vib. Vib.* **224**(1), 33–47 (1999)
- Huang, D., Zhou, S., Li, R., Yurchenko, D.: On the analysis of the tristable vibration isolation system with delayed feedback control under parametric excitation. *Mech. Syst. Signal Process.* **164**, 108207 (2022)
- Ghandchi Tehrani, M., Kalkowski, M.K.: Active control of parametrically excited systems. *J. Intell. Mater. Syst. Struct. Intell. Mater. Syst. Struct.* **27**(9), 1218–1230 (2016)
- Bauomy, H.S.: Active vibration control of a dynamical system via negative linear velocity feedback. *Nonlinear Dyn. Dyn.* **77**, 413–423 (2014)
- Chen, L.: Vibration and control of a parametrically excited mechanical system. In: *TENCON 2006–2006 IEEE Region 10 Conference*, pp. 1–4. IEEE (2006)
- Maccari, A.: Vibration control for parametrically excited Liénard systems. *Int. J. Nonlinear Mech.* **41**(1), 146–155 (2006)
- Zhao, Y.Y., Xu, J.: Using the delayed feedback control and saturation control to suppress the vibration of the dynamical system. *Nonlinear Dyn. Dyn.* **67**, 735–753 (2012)
- Chatterjee, S.: Vibration control by recursive time-delayed acceleration feedback. *J. Sound Vib. Vib.* **317**(1–2), 67–90 (2008)
- Fanson, J.L., Caughey, T.K.: Positive position feedback control for large space structures. *AIAA J.* **28**(4), 717–724 (1990)
- Sim, E., Lee, S.W.: Active vibration control of flexible structures with acceleration feedback. *J. Guid. Control. Dyn. Guid. Control. Dyn.* **16**(2), 413–415 (1993)
- Mondal, J., Chatterjee, S.: Controlling self-excited vibration of a nonlinear beam by nonlinear resonant velocity feedback with time-delay. *Int. J. Nonlinear Mech.* **131**, 103684 (2021)
- Dhobale, S.M., Chatterjee, S.: A general class of optimal nonlinear resonant controllers of fractional order with time-delay for active vibration control—theory and experiment. *Mech. Syst. Signal Process.* **182**, 109580 (2023)
- Abdelhafez, H., Nassar, M.: Effects of time delay on an active vibration control of a forced and Self-excited nonlinear beam. *Nonlinear Dyn. Dyn.* **86**, 137–151 (2016)
- Warminski, J., Cartmell, M.P., Mitura, A., Bochenski, M.: Active vibration control of a nonlinear beam with self- and external excitations. *Shock. Vib. Vib.* **20**(6), 1033–1047 (2013)
- Kamel, M., Kandil, A., El-Ganaini, W.A., Eissa, M.: Active vibration control of a nonlinear magnetic levitation system via nonlinear saturation controller (NSC). *Nonlinear Dyn. Dyn.* **77**, 605–619 (2014)
- Kandil, A., El-Gohary, H.A.: Suppressing the nonlinear vibrations of a compressor blade via a nonlinear saturation controller. *J. Vib. Control Vib. Control* **24**(8), 1488–1504 (2018)
- Gallacher, B.J., Burdess, J.S., Harish, K.M.: A control scheme for a MEMS electrostatic resonant gyroscope excited using combined parametric excitation and harmonic forcing. *J. Micromech. Microeng. Micromech. Microeng.* **16**(2), 320 (2006)
- Yabuno, H., Kanda, R., Lacarbonara, W., Aoshima, N.: Nonlinear active cancellation of the parametric resonance in a magnetically levitated body. *J. Dyn. Syst. Meas. Control* **126**(3), 433–442 (2004)
- Sahoo, P.K., Chatterjee, S.: High-frequency vibrational control of principal parametric resonance of a nonlinear cantilever beam: theory and experiment. *J. Sound Vib. Vib.* **505**, 116138 (2021)
- Sahoo, P.K., Chatterjee, S.: Nonlinear dynamics and control of galloping vibration under unsteady wind flow by high-frequency excitation. *Commun. Nonlinear Sci. Numer. Simul. Nonlinear Sci. Numer. Simul.* **116**, 106897 (2023)
- Cd, R., Cd, M.: Parametric control of flexible systems. *J. Vib. Acoust. Vib. Acoust.* **116**(3), 379–385 (1994)
- Senapati, R., Chatterjee, S.: Resonant dynamics of a single degree-of-freedom mechanical system under stiffness switching control with time-delay. *Int. J. Dyn. Control* **8**(2), 396–403 (2020)
- Chechurin, L., Mandrik, A., Vostrov, K., Chechurin, S.: Parametric and coordinate control of oscillating systems: physics-based oscillation feedback design. *IEEE Access* **9**, 113500–113507 (2021)
- Pumhossel, T., Ecker, H.: Active damping of vibrations of a cantilever beam by axial force control. In: *International Design Engineering Technical Conferences and Computers and Information in Engineering Conference*, vol. 48027, pp. 117–127 (2007)

28. Dimentberg, M.F., Bratus', A.S.: Bounded parametric control of random vibrations. Proc. Roy. Soc. Lond. Ser. A Math. Phys. Eng. Sci. **456**(2002), 2351–2363 (2000)
29. Chang, W., Jin, X., Huang, Z.: Optimal parametric control of nonlinear random vibrating systems. J. Vib. Acous. **143**, 4 (2021)
30. Strogatz, S.H.: Nonlinear Dynamics and Chaos with Student Solutions Manual: with Applications to Physics, Biology, Chemistry, and Engineering. CRC Press (2018)
31. Steve, S.I.U.: Let <https://www.mathworks.com/matlabcentral/fileexchange/233-let>, MATLAB Central File Exchange (2023). Retrieved 3 May 2023

Publisher's Note Springer Nature remains neutral with regard to jurisdictional claims in published maps and institutional affiliations.

Springer Nature or its licensor (e.g. a society or other partner) holds exclusive rights to this article under a publishing agreement with the author(s) or other rightsholder(s); author self-archiving of the accepted manuscript version of this article is solely governed by the terms of such publishing agreement and applicable law.